An unconditionally stable algorithm for generalized thermoelasticity based on operator-splitting and time-discontinuous Galerkin finite element methods

Mebratu F. Wakeni[a,b,*], B.D. Reddy[a,b], A.T. McBride[a,c]

[a] *Centre for Research in Computational and Applied Mechanics (CERECAM), University of Cape Town, 7701 Rondebosch, South Africa*
[b] *Department of Mathematics and Applied Mathematics, University of Cape Town, 7701 Rondebosch, South Africa*
[c] *Infrastructure and Environment School of Engineering, The University of Glasgow, Glasgow G12 8QQ*

Abstract

An efficient time-stepping algorithm is proposed based on operator-splitting and the space-time discontinuous Galerkin finite element method for problems in the non-classical theory of thermoelasticity. The non-classical theory incorporates three models: the classical theory based on Fourier's law of heat conduction resulting in a hyperbolic-parabolic coupled system, a non-classical theory of a fully-hyperbolic extension, and a combination of the two. The general problem is split into two contractive sub-problems, namely the mechanical phase and the thermal phase. Each sub-problem is discretized using the space-time discontinuous Galerkin finite element method. The sub-problems are stable which then leads to unconditional stability of the global product algorithm. A number of numerical examples are presented to demonstrate the performance and capability of the method.

Keywords: Operator-splitting, Space-time discontinuous Galerkin finite element, Non-classical theory of thermoelasticity, Fourier's law, Second sound.

1. Introduction

In some solids thermal energy can be transmitted by the mechanism of *wave-like* propagation of heat, unlike the usual mechanism of conduction by diffusion. This phenomenon of heat conduction as waves, known as *second sound*, has been observed experimentally (see, for example, [1, 2] for an extensive survey of experimental works involving propagation of heat as a thermal wave).

The classical theory of heat conduction based on *Fourier's law* fails to model the second sound phenomenon. Moreover, despite its success in broad range of applications, the classical theory permits *infinite speed* of propagation of parts of a localized initial heat pulse, which is paradoxical from a physical point of view. This drawback of the Fourier's law may be dominant in applications involving small scales at low ranges of temperature near absolute zero, leading to loss of validity [3]. As a result, efforts have been made to find a consistent model of heat propagation that is capable of capturing the second sound phenomenon with finite speed (see, for example, [4, 5] for a review of models of heat conduction as waves).

An alternative theory for formulating the propagation of heat in a general way that aims at capturing the second sound phenomenon was proposed by Green and Naghdi [6–9]. The theory of Green and Naghdi is based on three types of constitutive relations for the heat flux: Type I is equivalent to the classical theory based on Fourier's law. Type II permits the propagation of a localized heat signal as thermal wave without dissipation (see [10] for a remark on the appropriateness of this classification). Type III is the most general

*Corresponding author
Email address: wknmeb001@myuct.ac.za (Mebratu F. Wakeni)

theory, which includes both type I and II as special cases, in which second sound phenomenon is supported while dissipation is incorporated in the process.

The thermomechanical coupling of non-classical heat conduction with classical elasticity is the subject of non-classical thermoelasticity. Extensive overviews of the non-classical thermoelasticity theory of Green and Naghdi can be found in [4, 11, 12]. Theoretical results concerning the non-classical theory have been addressed in several research works. In [13] exact solutions are obtained for thermal wave propagation in one dimension. Results on the existence and uniqueness of solutions of the non-classical problem of thermoelasticity can be found, for example, in [14] and the references therein.

Designing a robust and efficient numerical solution strategy for strongly coupled problems of hyperbolic-type is challenging. This is particularly the case for the non-classical theory of thermoelasticity where the hyperbolic (or nearly hyperbolic) heat conduction equation is coupled with the classical hyperbolic elasticity problem. A standard approach for solving such time-dependent problems is the Method of Lines (MoL) in which the governing partial differential equation is first discretised in space using the finite element method (FEM) leading to a system of ordinary differential equations, which can then be solved using the finite difference method. Despite its popularity, MoL struggles to accurately solve problems involving propagation of sharp gradients or discontinuities [15, 16].

Recently, a great deal of attention has been invested in designing a spatial discontinuous Galerkin (DG) approach for convection-dominated problems; see for example [17]. However, these methods, like MoL, are based on decoupling space and time in the sense that space and time are treated differently. Hulbert and Hughes [15, 16] introduced a powerful scheme based on a space-time DG finite element methodology for linear elastodynamics problems. In their approach, space and time are treated simultaneously and the unknown fields are allowed to be discontinuous in time while continuous in space. Recently, the space-time DG method has been used in [18] for classical thermoelasticity, using a monolithic approach where all the unknown fields are solved for simultaneously.

In [19] a numerical solution approach based on MoL was proposed for non-classical thermoelasticity in which time integration was done in two ways: continuous Galerkin FEM for type II and III, while mixed-discountinuous Galerkin FEM for the classical problem based on the Fourier's law of heat conduction. A streamline-upwind numerical stabilization was added to localize numerical oscillations due to the propagation of sharp thermal wave.

In the current work, we extend the existence and uniqueness results otained in [14] for type II theory to the more general problem of type III thermoelasticity. We also present a novel numerical algorithm for the non-classical thermoelasticity based on an operator-splitting technique motivated by Armero and Simo [20] for classical thermoelasticity, coupled with a space-time DG methodology that extends the work of Hulbert and Hughes [15] which was formulated for linear elastodynamics. The major contributions of this work are two: (i) the adaptation of the operator-splitting strategy for classical thermoelasticity first proposed by [20] to the non-standard theory, in which the operator defining non-standard thermoelasticity is split in a way that the resulting sub-operators retain the same contractive behaviour as the global operator; and (ii) the development a time-DG formulation in which continuity of the unknown fields is enforced weakly by using an L^2-inner product in contrast to the energy-norm used in [15].

The rest of this paper is organized as follows. In Section 2, the governing equations of the non-classical theory are summarized in a general framework of type III thermoelasticity. Well-posedness and physically meaningful boundary and initial conditions are also discussed. An operator-splitting strategy for the problem of type II thermoelasticity is proposed and the resulting sub-operators are analysed in Section 3. In Section 4, a time-DG formulation is proposed for the sub-problems and stability of the individual algorithms and the global one is analysed. A number of numerical examples both in 1–D and 2–D are presented in Section 5 to demonstrate the excellent performance and capability of the proposed numerical scheme. Finally, concluding remarks and some open problems are discussed in Section 6.

2. Model problem: Non-classical thermoelasticity (type III)

This section summarizes the equations governing the non-classical theory of thermoelasticty of type III as proposed by Green and Naghdi. Well-posedness of the problem is analysed. Results obtained here will

serve as the basis for the design and analysis of the numerical algorithm that will be presented in later sections.

Governing equations

Let $\Omega \subset \mathbb{R}^d$, with $1 \leq d \leq 3$ be the reference placement of a continuum body $\mathcal{B}$ with smooth boundary Γ. Following Green and Naghdi's theory of thermoelasticity of type III, the system of partial differential equations governing the thermomechanical interaction in the solid $\mathcal{B}$ are

$$\left.\begin{aligned} \dot{\boldsymbol{u}} &= \boldsymbol{v} \\ \rho\dot{\boldsymbol{v}} &= \operatorname{div}[\mathbb{C}\boldsymbol{\varepsilon}(\boldsymbol{u}) - \mathbf{m}\vartheta] + \rho\mathbf{b} \\ \dot{\alpha} &= \Theta \\ \rho c\dot{\vartheta} &= \operatorname{div}[\mathbf{k}_2\nabla\alpha + \mathbf{k}_3\nabla\Theta] - \Theta_0\mathbf{m} : \boldsymbol{\varepsilon}(\dot{\boldsymbol{u}}) + \rho r \end{aligned}\right\} \text{ in } \Omega \times \mathbb{I}, \tag{1}$$

where $\mathbb{I} = [0,\ T]$ is the time interval of interest of length $T > 0$. Superimposed dots denote time derivatives. The displacement and the velocity vector fields are denoted by $\boldsymbol{u}$ and $\boldsymbol{v}$ respectively. The scalar field ϑ denotes the relative temperature with respect to a uniform reference value $\Theta_0 > 0$ such that the absolute temperature Θ is given by $\Theta = \vartheta + \Theta_0$. The quantities $\mathbf{b}$ and r are the prescribed body force and heat source.

Green and Naghdi's theory of non-classical thermoelasticity is based on the inclusion of a state variable, known as the *thermal displacement* α, that is defined in terms of an *empirical temperature* $\hat{T}$ (which is assumed to coincide with the absolute temperature Θ) through equation $(1)_3$, see, for example, [19, 21, 22] and the references therein.

The symbol $\boldsymbol{\varepsilon}(\boldsymbol{u}) = \operatorname{sym}(\nabla\boldsymbol{u})$ denotes the strain tensor associated with a displacement $\boldsymbol{u}$. It is assumed that the elasticity tensor $\mathbb{C}$ has the following properties:

$$\mathbb{C}_{ijkl} = \mathbb{C}_{jikl} = \mathbb{C}_{ijlk}, \tag{2}$$

$$\mathbb{C}_{ijkl} = \mathbb{C}_{klij}, \tag{3}$$

$$\mathbb{C}_{ijkl}\boldsymbol{\epsilon}_{ij}\boldsymbol{\epsilon}_{kl} > 0 \quad \text{for any non-zero symmetric tensor } \boldsymbol{\epsilon}. \tag{4}$$

Equations (2) and (3) are the minor and major symmetries of $\mathbb{C}$, while equation (4) is the positive definiteness of $\mathbb{C}$. The coupling second-order tensor $\mathbf{m}$ is of the form

$$\mathbf{m} = 3\omega\kappa\mathbf{1},$$

where ω, $\kappa = \lambda + 2/3\mu$, and $\mathbf{1}$ denote, respectively, the thermal expansion coefficient, the bulk modulus and the second-order identity tensor, and μ and λ are the Lamé constants. It is assumed that the tensor $\mathbf{k}_2$ is symmetric and positive-definite, and that $\mathbf{k}_3$ are symmetric and positive-semidefinite. In this paper, the material density $\rho > 0$ and the heat capacity $c > 0$ are assumed to be constants (however, in a more general case, they can be positive scalar functions on Ω).

Remarks:

1. The non-classical theory of thermoelasticity of type III (1) is the most general one in that it contains both type I and II as a special cases. If $\mathbf{k}_2\nabla\alpha$ is omitted from (1), then one obtains type I (or the classical thermoelastic model) where a parabolic heat conduction equation is coupled with the hyperbolic mechanical equation. On the other hand, if $\mathbf{k}_3$ is set to zero, one obtains type II thermoelastcity where part of the system (1), that is responsible for heat conduction, is hyperbolic (i.e. non-classical heat conduction).

2. Under the assumption of mechanical and thermal isotropy the elasticity tensor $\mathbb{C}$, and the tensors $\mathbf{k}_2$ and $\mathbf{k}_3$ become

$$\mathbb{C} = \lambda\mathbf{1}\otimes\mathbf{1} + 2\mu\mathbf{I}, \quad \mathbf{k}_2 = k_2\mathbf{1}, \quad \text{and} \quad \mathbf{k}_3 = k_3\mathbf{1},$$

where $\mathbf{I}$ denotes the fourth-order identity tensor, and $k_2 > 0$, and $k_3 \geq 0$ are constants.

3. The free energy per unit mass ψ, and hence the stress tensor $\boldsymbol{\sigma}$ and the entropy density η are given by

$$\begin{aligned}\rho\psi &= \frac{1}{2}\boldsymbol{\varepsilon} : \mathbb{C}\boldsymbol{\varepsilon} - \vartheta\mathbf{m} : \boldsymbol{\varepsilon} - \frac{1}{2}\frac{\rho c}{\Theta_0}\vartheta^2 - \vartheta S_0,\\ \boldsymbol{\sigma} &= \frac{\partial(\rho\psi)}{\partial\boldsymbol{\varepsilon}} = \mathbb{C}\boldsymbol{\varepsilon}(\boldsymbol{u}) - \mathbf{m}\vartheta,\\ \rho\eta &= -\frac{\partial(\rho\psi)}{\partial\Theta} = \frac{c\rho}{\Theta_0}\vartheta + \mathbf{m} : \boldsymbol{\varepsilon}(\boldsymbol{u}) + S_0,\end{aligned} \tag{5}$$

where S_0 is the absolute entropy density.

4. The heat flux vector $\boldsymbol{q}$ within the non-classical theory of thermoelasticity of type III is defined as

$$\boldsymbol{q} = -[\mathbf{k}_2\nabla\alpha + \mathbf{k}_3\nabla\Theta].$$

Using the entropy constitutive relation $(5)_3$ the coupled system (1) can be written in terms of η as

$$\left.\begin{aligned}\dot{\boldsymbol{u}} &= \boldsymbol{v}\\ \rho\dot{\boldsymbol{v}} &= \operatorname{div}[\mathbb{C}\boldsymbol{\varepsilon} - \mathbf{m}\vartheta] + \rho\mathbf{b}\\ \dot{\alpha} &= \Theta\\ \rho\Theta_0\dot{\eta} &= \operatorname{div}[\mathbf{k}_2\nabla\alpha + \mathbf{k}_3\nabla\Theta] + \rho r\end{aligned}\right\} \text{ in } \Omega\times[0,\ T]. \tag{6}$$

It is this form of the dynamical system which is crucial in designing the computational scheme based on operator-splitting in later sections.

2.1. Initial and boundary conditions

Let $\{\Gamma_{\boldsymbol{u}}, \Gamma_{\boldsymbol{t}}\}$ and $\{\Gamma_\vartheta, \Gamma_q\}$ be two partitions of Γ, each contains mutually disjoint subsets; that is,

$$\Gamma = \overline{\Gamma_{\boldsymbol{u}}\cup\Gamma_{\boldsymbol{t}}} = \overline{\Gamma_\vartheta\cup\Gamma_q},\ \text{with } \Gamma_{\boldsymbol{u}}\cap\Gamma_{\boldsymbol{t}} = \Gamma_\vartheta\cap\Gamma_q = \emptyset.$$

Let $\bar{\boldsymbol{u}} : \Gamma_{\boldsymbol{u}}\times\mathbb{I}\to\mathbb{R}^d$, $\bar{\boldsymbol{t}} : \Gamma_{\boldsymbol{t}}\times\mathbb{I}\to\mathbb{R}^d$, $\bar{\vartheta} : \Gamma_\vartheta\times\mathbb{I}\to\mathbb{R}$, and $\bar{q} : \Gamma_q\times\mathbb{I}\to\mathbb{R}$ be prescribed displacement, traction, thermal displacement and flux fields. Thus the boundary conditions are given by

$$\begin{aligned}\boldsymbol{u} &= \bar{\boldsymbol{u}} \quad \text{on} \quad \Gamma_{\boldsymbol{u}}\times\mathbb{I}, \qquad \vartheta = \bar{\vartheta} \quad \text{on} \quad \Gamma_\vartheta\times\mathbb{I},\\ \boldsymbol{\sigma}\mathbf{n} &= \bar{\boldsymbol{t}} \quad \text{on} \quad \Gamma_{\boldsymbol{t}}\times\mathbb{I}, \qquad \boldsymbol{q}\cdot\boldsymbol{n} = \bar{q} \quad \text{on} \quad \Gamma_q\times\mathbb{I},\end{aligned} \tag{7}$$

where $\boldsymbol{n}$ denotes the outward unit normal field to Γ. It is easy to observe the analogy between the two set of equations: the mechanical part $(1)_{1,2}$ and the thermal part $(1)_{3,4}$. In such analogy, we clearly see that the displacement $\boldsymbol{u}$ goes with the thermal displacement α (in fact, it is this analogy that motivated the name *thermal displacement* [6]), and the velocity $\boldsymbol{v}$ goes with the absolute temperature Θ, and hence with ϑ. As a consequence, however, one would expect a thermal Dirichlet boundary condition given in terms of α as is customarily the case in the mechanical part that $\boldsymbol{u}$ is prescribed as a Dirchlet boundary condition. The thermal Dirichlet boundary condition, in this case, is given via the relative temperature ϑ (and hence absolute temperature Θ). The reason for this is that, usually, boundary conditions are prescribed in terms of physical quantities, which can be measured, which, in the thermal case, is the relative temperature, ϑ (or Θ).

Furthermore, the initial conditions read

$$\begin{aligned}\boldsymbol{u}(\mathbf{x},0) &= \boldsymbol{u}^0(\mathbf{x}), \quad \boldsymbol{v}(\mathbf{x},0) = \boldsymbol{v}^0(\mathbf{x}),\\ \alpha(\mathbf{x},0) &= \alpha^0(\mathbf{x}), \quad \vartheta(\mathbf{x},0) = \vartheta^0(\mathbf{x}),\end{aligned} \tag{8}$$

where $\boldsymbol{u}^0$, $\boldsymbol{v}^0$, α^0, and ϑ^0 are prescribed initial displacement, velocity, thermal displacement and absolute temperature respectively. In prescribing an initial thermal state, a thermal configuration is assumed so that the initial thermal displacement α is homogeneous, that is $\alpha^0 = 0$, while, the experimentally observable quantity, the relative temperature can be initiated at a non-zero value. The existence of such state is a constitutive assumption that is related to the notion of natural configuration.

2.2. Well-posedness: Dissipation and conservation

Let L_c, T_c, M_c, and K_c be characteristic scalar quantities with the dimensions of length, time, mass, and temperature, respectively. Define the dimensionless variables as

$$\bar{\boldsymbol{u}} = \left[\frac{1}{L_c}\right]\mathbf{u}, \qquad \bar{\boldsymbol{v}} = \left[\frac{T_c}{L_c}\right]\boldsymbol{v}, \qquad \bar{\boldsymbol{x}} = \left[\frac{1}{L_c}\right]\boldsymbol{x}, \qquad \bar{t} = \left[\frac{1}{T_c}\right]t,$$
$$\bar{\Theta} = \left[\frac{1}{K_c}\right]\Theta, \qquad \bar{\alpha} = \left[\frac{1}{T_c K_c}\right]\alpha, \qquad \bar{\rho} = \left[\frac{L_c^3}{M_c}\right]\rho, \qquad \bar{\Theta}_0 = \left[\frac{1}{K_c}\right]\Theta_0.$$

After introducing the dimensionless variables, the non-dimensional form of (1) become

$$\begin{aligned} \dot{\bar{\boldsymbol{u}}} &= \bar{\boldsymbol{v}}, \\ \rho\dot{\bar{\boldsymbol{v}}} &= \operatorname{div}[\bar{\mathbb{C}}\boldsymbol{\varepsilon}(\bar{\boldsymbol{u}}) - \bar{\mathbf{m}}\bar{\vartheta}] + \bar{\rho}\bar{\mathbf{b}}, \\ \dot{\bar{\alpha}} &= \bar{\Theta}, \\ \bar{\rho}\bar{c}\dot{\bar{\Theta}} &= \operatorname{div}[\bar{\mathbf{k}}_2\nabla\bar{\alpha} + \bar{\mathbf{k}}_3\nabla\bar{\Theta}] - \bar{\Theta}_0\bar{\mathbf{m}} : \boldsymbol{\varepsilon}(\dot{\bar{\boldsymbol{u}}}) + \bar{\rho}\bar{r}, \end{aligned} \tag{9}$$

where the spatial and time derivatives are with respect to the dimensionless space and time variables, and

$$\bar{\mathbb{C}} = \left[\frac{L_c T_c^2}{M_c}\right]\mathbb{C}, \qquad \bar{\mathbf{m}} = \left[\frac{L_c T_c^2 K_c}{M_c}\right]\mathbf{m}, \qquad \bar{\boldsymbol{b}} = \left[\frac{T_c^2}{L_c}\right]\boldsymbol{b}, \qquad \bar{c} = \left[\frac{K_c T_c^2}{L_c^2}\right]c,$$
$$\bar{\mathbf{k}}_2 = \left[\frac{T_c^4 K_c}{M_c L_c}\right]\mathbf{k}_2, \qquad \bar{\mathbf{k}}_3 = \left[\frac{T_c^3 K_c}{M_c L_c}\right]\mathbf{k}_3, \qquad \bar{r} = \left[\frac{T_c^3}{L_c^2}\right]r.$$

If we drop the bars in the notations of equation (9), similar expressions as in equation (1) are obtained. For the remainder of this section, whenever the system (1) is mentioned, unless stated otherwise, it refers to its non-dimensional form, and the initial and boundary conditions should also be understood accordingly.

The positive-definiteness property of $\mathbb{C}$ and $\mathbf{k}_2$, and the positive-semidefinite-ness of $\mathbf{k}_3$ imply that the system (1) together with the initial and boundary conditions (7) and (8) define an evolution equation of a general form

$$\left.\begin{aligned} \dot{\boldsymbol{\chi}}(t) &= \mathbf{A}\boldsymbol{\chi}(t) + \mathbf{f} \\ \boldsymbol{\chi}(0) &= \boldsymbol{\chi}^0 \end{aligned}\right\} \quad \text{in } \mathcal{V}, \tag{10}$$

where $\mathbf{A}$ is a closed linear operator with dense domain $\mathcal{D}(\mathbf{A}) \subset \mathcal{V}$ defined in some suitable Banach space $\mathcal{V}$. For the case of non-classical linear thermoelasticity, for the sake of simplicity, we consider homogeneous Dirichlet boundary conditions with respect to both $\boldsymbol{u}$ and α and the space $\mathcal{V}$ defined

$$\mathcal{V} := \left\{(\boldsymbol{u}, \boldsymbol{v}, \alpha, \Theta)^T \in [\mathbf{H}^1(\Omega)]^d \times [L^2(\Omega)]^d \times \mathbf{H}^1(\Omega) \times L^2(\Omega) : \boldsymbol{u} = \mathbf{0}, \alpha = 0 \text{ on } \Gamma\right\}, \tag{11}$$

is a Hilbert space.

The abstract solution vector $\boldsymbol{\chi} = (\boldsymbol{u}, \boldsymbol{v}, \alpha, \Theta) \in \mathcal{V}$, while the linear operator $\mathbf{A}$ and the source term $\mathbf{f}$ in (10) are defined by

$$\mathbf{A}\boldsymbol{\chi} := \begin{bmatrix} \boldsymbol{v} \\ \frac{1}{\rho}\operatorname{div}[\mathbb{C}\boldsymbol{\varepsilon}(\boldsymbol{u}) - \mathbf{m}\vartheta] \\ \Theta \\ \frac{1}{\rho c}\operatorname{div}[\mathbf{k}_2\nabla\alpha + \mathbf{k}_3\nabla\Theta] - \frac{\Theta_0}{\rho c}\mathbf{m} : \boldsymbol{\varepsilon}(\boldsymbol{v}) \end{bmatrix}, \quad \mathbf{f} := \begin{bmatrix} \mathbf{0} \\ \boldsymbol{b} \\ 0 \\ \frac{1}{c}r \end{bmatrix}. \tag{12}$$

We consider an inner product, $\langle\cdot,\cdot\rangle_{\mathcal{V}}$ on $\mathcal{V}$ defined by

$$\langle\boldsymbol{\chi}, \bar{\boldsymbol{\chi}}\rangle_{\mathcal{V}} = \langle\boldsymbol{\varepsilon}(\boldsymbol{u}), \mathbb{C}\boldsymbol{\varepsilon}(\bar{\boldsymbol{u}})\rangle + \langle\rho\boldsymbol{v}, \bar{\boldsymbol{v}}\rangle + \langle\mathbf{k}_2^*\nabla\alpha, \nabla\bar{\alpha}\rangle + \left\langle c^*\vartheta, \bar{\vartheta}\right\rangle. \tag{13}$$

where $\langle \cdot, \cdot \rangle$ denotes the standard L^2-inner product pairing of tensor, vector, or scalar fields, that should be understood in context, and $\mathbf{k}_2^* = \mathbf{k}_2 \rho c/\Theta_0$ and $c^* = \rho c/\Theta_0$. The norm on $\mathcal{V}$ induced by the inner product $\langle \cdot, \cdot \rangle_{\mathcal{V}}$ is denoted by $\| \cdot \|_{\mathcal{V}}$.

Note that the linear differential operator $\mathbf{A} : \mathcal{D}(\mathbf{A}) \subset \mathcal{V} \to \mathcal{V}$ is closed and the space

$$[\mathbf{H}_0^1(\Omega) \cap \mathbf{H}_0^2(\Omega)]^d \times [\mathbf{H}_0^1(\Omega)]^d \times (H_0^1(\Omega) \cap H_0^2(\Omega)) \times H_0^1(\Omega) \subset \mathcal{D}(\mathbf{A}), \tag{14}$$

is dense in $\mathcal{V}$. Hence $\mathcal{D}(\mathbf{A})$ is dense in $\mathcal{V}$.

A very important inequality concerning the evolution equation (10) relates to the *dissipativity property* of the defining operator $\mathbf{A}$. An operator $\mathbf{A}$ on closed subspace $\mathcal{D}(\mathbf{A})$ of a Hilbert space $\mathcal{V}$ endowed with an inner product $\langle \cdot, \cdot \rangle_{\mathcal{V}}$ is said to be dissipative if it satisfies the inequality $\langle \mathbf{A}\boldsymbol{\chi}, \boldsymbol{\chi} \rangle_{\mathcal{V}} \leq 0$ for each $\boldsymbol{\chi} \in \mathcal{D}(\mathbf{A})$ [20]. If the operator $\mathbf{A}$ is dissipative, the norm of the solution of the corresponding evolution equation is monotonically decreasing in time, which is referred to as *contractivity* of the solution. That is, for a solution $\boldsymbol{\chi}$ of the evolution problem (10), assuming dissipativity of $\mathbf{A}$ and $\mathbf{f} = \mathbf{0}$, we have

$$\frac{d}{dt}\|\boldsymbol{\chi}\|_{\mathcal{V}} = \frac{d}{dt}\langle \boldsymbol{\chi}, \boldsymbol{\chi} \rangle_{\mathcal{V}} = 2\langle \dot{\boldsymbol{\chi}}, \boldsymbol{\chi} \rangle_{\mathcal{V}} = 2\langle \mathbf{A}\boldsymbol{\chi}, \boldsymbol{\chi} \rangle \leq 0. \tag{15}$$

Now, we shall show that the operator $\mathbf{A}$ that defines the problem (10) is dissipative. Let $\boldsymbol{\chi} = (\boldsymbol{u}, \boldsymbol{v}, \alpha, \vartheta)^T$ be in the domain of $\mathbf{A}$, $\mathcal{D}(\mathbf{A})$, satisfying the homogeneous boundary condition. Then

$$\begin{aligned}
\langle \boldsymbol{\chi}, \mathbf{A}\boldsymbol{\chi} \rangle_{\mathcal{V}} &= \langle \boldsymbol{\varepsilon}(\boldsymbol{u}), \mathbb{C}\boldsymbol{\varepsilon}(\mathbf{v}) \rangle + \langle \rho \mathbf{v}, \frac{1}{\rho}\mathrm{div}[\mathbb{C}\boldsymbol{\varepsilon}(\boldsymbol{u}) - \mathbf{m}\vartheta \rangle \\
&\quad + \langle \mathbf{k}_2^* \nabla\alpha, \nabla\Theta \rangle + \langle c^*\vartheta, \frac{1}{\rho c}\mathrm{div}[\mathbf{k}_2\nabla\alpha + \mathbf{k}_3\nabla\Theta] - \frac{\Theta_0}{c}\mathbf{m} : \boldsymbol{\varepsilon}(\boldsymbol{v}) \rangle \\
&= \langle \boldsymbol{\varepsilon}(\boldsymbol{u}), \mathbb{C}\boldsymbol{\varepsilon}(\boldsymbol{v}) \rangle - \langle \boldsymbol{\varepsilon}(\boldsymbol{v}), \mathbb{C}\boldsymbol{\varepsilon}(\boldsymbol{u}) \rangle + \langle \boldsymbol{\varepsilon}(\boldsymbol{v}), \mathbf{m}\vartheta \rangle + \langle \frac{\rho c}{\Theta_0}\mathbf{k}_2\nabla\alpha, \nabla\Theta \rangle \\
&\quad - \langle \frac{\rho c}{\Theta_0}\mathbf{k}_2\nabla\Theta, \nabla\alpha \rangle - \langle \frac{\rho c}{\Theta_0}\mathbf{k}_3\nabla\Theta, \nabla\Theta \rangle - \langle \vartheta, \mathbf{m} : \boldsymbol{\varepsilon}(\boldsymbol{v}) \rangle \\
&= -\langle \frac{\rho c}{\Theta_0}\mathbf{k}_3\nabla\Theta, \nabla\Theta \rangle \leq 0.
\end{aligned} \tag{16}$$

In the general, since $\mathbf{k}_3$ is positive-semidefinite equation (16) leads to dissipation. In the limiting case where $\mathbf{k}_3 = \mathbf{0}$ (type II) the above argument implies conservation of energy-norm

$$\mathscr{E}(t) := \|\boldsymbol{\chi}\|_{\mathcal{V}}^2 = \frac{1}{2}\int_\Omega [\boldsymbol{\varepsilon}(\boldsymbol{u}) : \mathbb{C}\boldsymbol{\varepsilon}(\boldsymbol{u}) + \rho \boldsymbol{v} \cdot \boldsymbol{v} + \mathbf{k}_2^* \nabla\alpha \cdot \nabla\alpha + c^*\vartheta^2]\mathrm{d}\Omega. \tag{17}$$

This is the reason why type II is also referred to as the theory of thermoelasticity *without energy dissipation*, see, for example, [6, 8, 14].

Another important property of the operator $\mathbf{A}$ is that it should satisfy the following: for all $\boldsymbol{\chi}^* \in \mathcal{V}$, there exists $\boldsymbol{\chi}$ in $\mathcal{D}(\mathbf{A})$ such that

$$\boldsymbol{\chi} - \mathbf{A}\boldsymbol{\chi} = \boldsymbol{\chi}^*, \tag{18}$$

in other words, the operator $(\mathbf{1} - \mathbf{A}) : \mathcal{D}(\mathbf{A}) \to \mathcal{V}$ is onto.

To show that $\mathbf{A}$ satisfies the relation (18), we proceed as follows: let $\boldsymbol{\chi} = (\boldsymbol{u}, \boldsymbol{v}, \alpha, \vartheta)^T$ and $\boldsymbol{\chi}^* = (\boldsymbol{u}^*, \boldsymbol{v}^*, \alpha^*, \vartheta^*)^T$ then from the definition of $\mathbf{A}$ equation (18), implies that

$$\begin{aligned}
\boldsymbol{u} - \boldsymbol{v} &= \boldsymbol{u}^*, \\
\boldsymbol{v} - \frac{1}{\rho}\mathrm{div}[\mathbb{C}\boldsymbol{\varepsilon}(\boldsymbol{u}) - \mathbf{m}\vartheta] &= \boldsymbol{v}^*, \\
\alpha - \vartheta &= \alpha^*, \\
\vartheta - \frac{1}{\rho c}\mathrm{div}[\mathbf{k}_2\nabla\alpha + \mathbf{k}_3\nabla\Theta] + \frac{\Theta_0}{c}\mathbf{m} : \boldsymbol{\varepsilon}(\boldsymbol{v}) &= \vartheta^*.
\end{aligned} \tag{19}$$

Substitution of equations $(19)_1$ and $(19)_3$ into the remaining equations of (19) leads to the (equilibrium) problem: find $\boldsymbol{\chi} = (\boldsymbol{u}, \boldsymbol{v}, \alpha, \vartheta)^T \in \mathcal{D}(\mathbf{A})$ such that $\boldsymbol{v} = \boldsymbol{u} - \boldsymbol{u}^*$, $\vartheta = \alpha - \alpha^*$ and satisfying

$$\begin{aligned} \rho^2\Theta_0\boldsymbol{u} - \rho\Theta_0\mathrm{div}[\mathbb{C}\boldsymbol{\varepsilon}(\boldsymbol{u}) - \mathbf{m}\alpha] &= \mathring{\boldsymbol{u}}, \\ \rho c\alpha - \mathrm{div}[\mathbf{k}\nabla\alpha] + \rho\Theta_0\mathbf{m} : \boldsymbol{\varepsilon}(\boldsymbol{u}) &= \mathring{\alpha}, \end{aligned} \tag{20}$$

where $\mathring{\boldsymbol{u}} = \rho^2\Theta_0\boldsymbol{u}^* + \rho^2\Theta_0\boldsymbol{v}^* + \rho\Theta_0\mathrm{div}[\mathbf{m}\alpha^*]$, $\mathring{\alpha} = \rho c\alpha^* + \rho c\vartheta^* - \mathrm{div}[\mathbf{k}_3\nabla\alpha^*] + \rho\Theta_0\mathbf{m} : \boldsymbol{\varepsilon}(\boldsymbol{u}^*)$, and $\mathbf{k} = \mathbf{k}_2 + \mathbf{k}_3$.

The weak form of equation (20) reads: find $\boldsymbol{\chi} = (\boldsymbol{u}, \boldsymbol{v}, \alpha, \vartheta)^T \in \mathcal{V}$ such that $\boldsymbol{v} = \boldsymbol{u} - \boldsymbol{u}^*$, $\vartheta = \alpha - \alpha^*$ and satisfying

$$B(\boldsymbol{\chi}, \boldsymbol{\xi}) = l(\boldsymbol{\xi}) \tag{21}$$

for all $\boldsymbol{\xi} = (\boldsymbol{w}, \boldsymbol{\nu}, \beta, \varpi) \in \mathcal{V}$. The bilinear form $B(\cdot,\ \cdot)$ and the right hand side functional $l(\cdot)$ are given by

$$\begin{aligned} B(\boldsymbol{\chi}, \boldsymbol{\xi}) = {} & \langle \rho^2\Theta_0\boldsymbol{u}, \boldsymbol{w}\rangle + \langle \rho\Theta_0\mathbb{C}\boldsymbol{\varepsilon}(\boldsymbol{u}), \boldsymbol{\varepsilon}(\boldsymbol{w})\rangle - \langle \rho\Theta_0\mathbf{m}\alpha, \varepsilon(\boldsymbol{w})\rangle \\ & + \langle \rho c\alpha, \beta\rangle + \langle \mathbf{k}\nabla\alpha, \nabla\beta\rangle + \langle \rho\Theta_0\mathbf{m} : \boldsymbol{\varepsilon}(\boldsymbol{u}), \beta\rangle, \qquad (22) \\ l(\boldsymbol{\xi}) = {} & \langle \mathring{\boldsymbol{u}}, \boldsymbol{w}\rangle + \langle \mathring{\alpha}, \beta\rangle. \qquad (23) \end{aligned}$$

Note that $\mathring{\boldsymbol{u}} \in [\mathbf{H}^{-1}(\Omega)]^d$ and $\mathring{\alpha} \in \mathbf{H}^{-1}(\Omega)$ and here the symbol $\langle\cdot,\cdot\rangle$ in equation (23) represents duality pairing in their respective spaces.

From the definition of $B(\cdot,\cdot)$, we can easily see that it is a bounded bilinear form. Since

$$B(\boldsymbol{\chi}, \boldsymbol{\chi}) = \langle \rho^2\Theta_0\boldsymbol{u}, \boldsymbol{u}\rangle + \langle \rho\Theta_0\mathbb{C}\boldsymbol{\varepsilon}(\boldsymbol{u}), \boldsymbol{\varepsilon}(\boldsymbol{u})\rangle + \langle \rho c\alpha, \alpha\rangle + \langle \mathbf{k}\nabla\alpha, \nabla\alpha\rangle, \tag{24}$$

then $B(\cdot,\cdot)$ is $([\mathbf{H}_0^1(\Omega)]^d \times \mathbf{H}_0^1(\Omega))$-elliptic. By applying Lax-Milgram theorem we conclude that there exists $\boldsymbol{\chi} \in \mathcal{V}$ which solves the weak problem (21), and hence solves equation (19). Therefore, this proves the ontoness of the resolvent operator $(\mathbf{1} - \mathbf{A})$.

In conclusion, we have shown that the operator $\mathbf{A}$ defining the non-classical linear thermoelasticity (type III)

i) is closed,

ii) has dense domain $\mathcal{D}(\mathbf{A})$ in $\mathcal{V}$,

iii) is dissipative, and

iv) is such that $(\mathbf{1} - \mathbf{A}) : \mathcal{D}(\mathbf{A}) \subset \mathcal{V} \to \mathcal{V}$ is onto.

Therefore, by the Lumer-Phillips theorem, $\mathbf{A}$ generates a strongly continuous semigroup of contractions in $\mathcal{V}$, see, for example [14] and the references therein. In other words, the problem (10) is well-defined and contractive. This also means that the dynamical system represented by the equation of non-classical thermoelasticity of type III is, in general, stable in the sense of Lyapunov.

3. Algorithms based on operator-splitting strategy

Consider an abstract evolutionary problem of the form (10). Assume that $\mathbf{A}$ can be expressed additively as

$$\mathbf{A} = \mathbf{A}_1 + \mathbf{A}_2 \tag{25}$$

such that the operators $\mathbf{A}_i$, $i = 1, 2$ define sub-problems

$$\dot{\boldsymbol{\chi}}_i = \mathbf{A}_i\boldsymbol{\chi}\,; \quad \boldsymbol{\chi}_i(0) = \boldsymbol{\chi}_i^0, \quad i = 1, 2. \tag{26}$$

Let $\mathbb{A}_i^{\Delta t}$ be consistent and stable time-stepping algorithms corresponding to the sub-problems (26) with Δt the time step length over which the algorithms evolve the state vectors, $\boldsymbol{\chi}_i$, from a given time t to $t + \Delta t$. A time-stepping algorithm, $\mathbb{A}^{\Delta t}$, for the global problem is obtained by taking products of the algorithms

$$\mathbb{A}^{\Delta t} = \mathbb{A}_2^{\Delta t} \circ \mathbb{A}_1^{\Delta t}, \tag{27}$$

The algorithm $\mathbb{A}^{\Delta t}$ is referred to as *Lie-Trotter-Kato product formula* [23]. It is sometimes called a *sequential split algorithm* or *single pass algorithm*. In addition to the discretization error in the individual algorithms $\mathbb{A}_i^{\Delta t}$, the application of the operator-splitting strategy introduces another source of error known as the *splitting error*. The splitting error associated to the Lie-Trotter-Katto product formula (27) is of order of magnitude $\mathcal{O}(\Delta t)$ (see, for example, [24]). It means that $\mathbb{A}^{\Delta t}$ is only first order accurate. Higher-order algorithms based on operator-splitting strategies include:

$$\begin{aligned} &\text{Marchuk-Strang split:} && \mathbb{A}^{\Delta t} = \mathbb{A}_1^{\Delta t/2} \circ \mathbb{A}_2^{\Delta t} \circ \mathbb{A}_1^{\Delta t/2} \\ &\text{Double-pass split:} && \mathbb{A}^{\Delta t} = \frac{1}{2}(\mathbb{A}_2^{\Delta t} \circ \mathbb{A}_1^{\Delta t} + \mathbb{A}_1^{\Delta t} \circ \mathbb{A}_2^{\Delta t}). \end{aligned} \tag{28}$$

The Marchuk–Strang split is second-order accurate, while the double-pass split is only first-order. Note that Lie-Trotter-Kato product formula depends on the order of operations, for example in (27), $\mathbb{A}_1^{\Delta t}$ is applied first followed by $\mathbb{A}_2^{\Delta t}$, while the order of operations does not matter in the other two operator-splitting algorithms given in (28).

Remarks:

1. Perhaps the main reason why operator-splitting schemes might be advantageous over a monolithic approach is in the case of coupled problems involving different classes of sub-problems. Such multi-physics problems can be handled in a quite natural way which allows to use different classes of methods to efficiently solve each sub-problems so that they can be joined together in a suitable way to form the global algorithms. Such splitting schemes can be very important, for example, in problems involving interaction of fluid and structure.

2. Splitting schemes can be constructed for coupled problems exhibiting multiple time scales. In such cases, the faster dynamics is solved, with-in a time-step, several times with fraction of the full time-step, while the slower dynamics is solved in a larger portion of the time-step depending on its scale. The schemes for each component should be sufficiently accurate for the global algorithm to be useful. In fact, the mechanism of capturing different time scales is natural in splitting schemes. Whereas, a standard monolithic scheme only admits a single time-step which depend on of scale of the fastest component.

3. Splitting schemes are very suitable for parallel computing. It will be shown in the remainder of this paper that an operator-splitting strategy for generalized thermoelasticity is considered. In this split, it will be shown that an entropy controlling mechanism helps to effectively decoupled the resulting two problems which can be solved simultaneously, which is a recipe for paralliziation.

4. One of the limiting factors of splitting schemes is that it is very difficult to construct schemes which are higher than second-order. However, the design of higher order p- and hp-adaptive schemes are possible with monolithic schemes.

5. Operator-splitting is not always possible, especially if the coupling between the physical phenomenon represented in two or more systems is too strong. In this case, the monolithic approach is the only possible feasible method.

3.1. Operator-splitting for non-classical thermoelasticity

The non-classical theory of thermoelasticity is a coupling of two dynamical systems: the classical linear elasticity and the non-Fourier thermal conduction. A naive splitting of the system (1) into a mechanical problem under constant thermal states (isothermal) and a thermal problem with a fixed configuration will result in at most a conditionally stable algorithm even if the sub-algorithms for the two processes are unconditionally stable. Considerable care must be taken in splitting the two systems; this is usually dictated by an understanding of the underlying physics. In this respect, it makes sense to split the operator $\mathbf{A}$ in (12) so that in the mechanical phase the entropy is held fixed (isentropic) while the temperature is allowed to vary, and in the thermal phase heat is allowed to be conducted while the configuration is fixed. In fact, for this split, it can be shown that each sub-process defines an evolution problem which is contractive, as is the global problem. Furthermore, consistent and stable algorithms for the sub-processes render a consistent and stable algorithm for the global problem by the way of operator-splitting strategy.

To this end, inspired by the work of Armero and Simo [20], taking the 4-tuple $\boldsymbol{\Sigma} = (\boldsymbol{u}, \boldsymbol{v}, \alpha, \eta)^T$ as the state variables we consider the splitting of the system of equation (1) into

$$\begin{cases} \dot{\boldsymbol{u}} = \boldsymbol{v}, \\ \rho\dot{\boldsymbol{v}} = \operatorname{div}[\mathbb{C}\boldsymbol{\varepsilon}(\boldsymbol{u}) - \mathbf{m}\vartheta] + \rho\mathbf{b}, \\ \dot{\alpha} = 0, \\ \rho\Theta_0\dot{\eta} = 0, \end{cases} \quad \text{and} \quad \begin{cases} \dot{\boldsymbol{u}} = 0, \\ \rho\dot{\boldsymbol{v}} = 0, \\ \dot{\alpha} = \Theta, \\ \rho\Theta_0\dot{\eta} = \operatorname{div}[\mathbf{k}_2\nabla\alpha + \mathbf{k}_3\nabla\Theta] + \rho r. \end{cases} \tag{29}$$

This corresponds to the additive splitting of the operator $\mathbf{A} = \mathbf{A}_1 + \mathbf{A}_2$ in (10)

$$\mathbf{A}_1\boldsymbol{\Sigma} = \begin{bmatrix} \boldsymbol{v} \\ \dfrac{1}{\rho}\operatorname{div}[\mathbb{C}\boldsymbol{\varepsilon}(\boldsymbol{u}) - \mathbf{m}\vartheta] \\ 0 \\ 0 \end{bmatrix}, \qquad \mathbf{A}_2\boldsymbol{\Sigma} = \begin{bmatrix} \mathbf{0} \\ \mathbf{0} \\ \Theta \\ \dfrac{1}{\rho c}\operatorname{div}[\mathbf{k}_2\nabla\alpha + \mathbf{k}_3\nabla\Theta] \end{bmatrix}. \tag{30}$$

Using the same calculation as for the dissipativity of $\mathbf{A}$ in (16), we obtain the estimates such that for each $\boldsymbol{\Sigma}$,

$$\begin{aligned} \langle \mathbf{A}_1\boldsymbol{\Sigma}, \boldsymbol{\Sigma}\rangle_{\mathcal{V}} &= 0, \\ \langle \mathbf{A}_2\boldsymbol{\Sigma}, \boldsymbol{\Sigma}\rangle_{\mathcal{V}} &= -\langle \frac{\rho c}{\Theta_0}\mathbf{k}_3\nabla\Theta, \nabla\Theta\rangle \leq 0. \end{aligned} \tag{31}$$

In the general case, since $\mathbf{k}_3$ is positive-semidefinite, both operators $\mathbf{A}_1$ and $\mathbf{A}_2$ are dissipative. In particular, if $\mathbf{k}_3 = 0$, the systems that accounts for thermal conduction, $(29)_2$, is energy conserving, i.e. it represents heat conduction without energy loss in a rigid body. Moreover, it can be shown that both of the sub-operators satisfy additional conditions in order to generate strongly continuous semigroups of contraction just like what is done in Section 2.2.

Now, having two sub-operators $\mathbf{A}_1$ and $\mathbf{A}_2$ generating contractive semigroups, assume that there corresponds two algorithms $\mathbb{A}_i^{\Delta t}$, $i = 1, 2$ which are *B-stable* (*non-linearly stable*); that is

$$\|\mathbb{A}_i^{\Delta t}\boldsymbol{\chi}^n - \mathbb{A}_i^{\Delta t}\tilde{\boldsymbol{\chi}}\| \leq \|\boldsymbol{\chi}^n - \tilde{\boldsymbol{\chi}}\| \quad \text{for all } \boldsymbol{\chi}^n,\ \tilde{\boldsymbol{\chi}} \in \mathcal{V}. \tag{32}$$

In the linear case this means that each of the algorithms satisfy the estimate (see [20, 25] and the references therein):

$$\|\mathbb{A}_i^{\Delta t}\|_{\mathcal{V}^*} \leq 1, \qquad i = 1, 2. \tag{33}$$

where $\mathcal{V}^*$ is the dual of $\mathcal{V}$. Let $\{\boldsymbol{\chi}^n\}_{n\in\mathbb{N}}$ and $\{\tilde{\boldsymbol{\chi}}^n\}_{n\in\mathbb{N}}$ be two sequences in $\mathcal{V}$ generated by the Lie-Trotter-Kato product formula $\mathbb{A}^{\Delta t}$ corresponding to two initial conditions $\boldsymbol{\chi}(0) = \boldsymbol{\chi}^0$ and $\tilde{\boldsymbol{\chi}}(0) = \tilde{\boldsymbol{\chi}}^0$ respectively.

Then the product formula $\mathbb{A}^{\Delta t}$ satisfies the stability estimate

$$\begin{aligned}\|\boldsymbol{\chi}^{n+1}-\tilde{\boldsymbol{\chi}}^{n+1}\|_{\mathcal{V}} &= \|\mathbb{A}^{\Delta t}\boldsymbol{\chi}^{n}-\mathbb{A}^{\Delta t}\tilde{\boldsymbol{\chi}}^{n}\|_{\mathbf{V}}\\ &= \|\mathbb{A}_2^{\Delta t}[\mathbb{A}_1^{\Delta t}\boldsymbol{\chi}^{n}]-\mathbb{A}_2^{\Delta t}[\mathbb{A}_1^{\Delta t}\tilde{\boldsymbol{\chi}}^{n}\|_{\mathcal{V}}\\ &\leq \|\mathbb{A}_1^{\Delta t}\boldsymbol{\chi}^{n}-\mathbb{A}_1^{\Delta t}\tilde{\boldsymbol{\chi}}^{n}\|_{\mathcal{V}} \qquad (\|\mathbb{A}_2^{\Delta t}\|_{\mathcal{V}}\leq 1)\\ &= \|\boldsymbol{\chi}^{n}-\tilde{\boldsymbol{\chi}}^{n}\|_{\mathcal{V}} \qquad (\|\mathbb{A}_1^{\Delta t}\|_{\mathcal{V}}\leq 1),\end{aligned} \tag{34}$$

which proves the *non-linear stability* of the global algorithm corresponding to the product formula $\mathbb{A}^{\Delta t}$.

The numerical scheme formulated in the subsequent sections is based on the operator-splitting approach and time-discontinuous Galerkin finite element method. A Lie-Trotter-Kato product formula is applied to merge algorithms for the two phases. Hence, the product formula can also be viewed in the sense of a *predictor–corrector* scheme, where the sub-algorithm for the mechanical phase is used as predictor and that of the thermal phase as a corrector.

4. Time-discontinuous Galerkin finite element method

Let $\boldsymbol{T}_h = \{\Omega^e\}$ be a triangulation of $\bar{\Omega}$, where $\bar{\Omega}$ denotes the closure (the union of the interior and boundary) of Ω, such that

$$\bar{\Omega} = \bigcup_{\Omega^e\in\boldsymbol{T}_h}\Omega^e. \tag{35}$$

Denote the space of scalar piecewise polynomials on the mesh $\boldsymbol{T}_h$ by $\mathscr{P}_h^j$:

$$\mathscr{P}_h^j = \left\{\varphi_{_h}\in C^0(\bar{\Omega}) : \varphi_{_h}|_{_{\Omega^e}}\in P^j(\Omega^e),\ \Omega^e\in\boldsymbol{T}_h\right\}, \tag{36}$$

where $P^j(\Omega^e)$ denotes the set of polynomials of degree at most j defined on Ω^e.

Consider a partition of the time domain $\mathbb{I}=[0,T]$ into the collection $\{I_n=[t_n,t_{n+1}]\}_{n=0}^{N-1}$, $N\in\mathbb{N}$ of non-overlapping subintervals. The time step length is $\Delta t_n = t_{n+1}-t_n$ for $n=0,1,\cdots,N-1$ with

$$0=t_0<t_1<\cdots<t_N=T.$$

For each time sub-domain I_n we consider the space-time domain of the form $Q_n=\bar{\Omega}\times I_n$ referred to as the n^{th} *space-time slab*.

Admissible scalar functions, ϕ^h, that we consider in the time time-discontinuous Galerkin finite element (T-DG FEM) formulation will be polynomials in time $t\in I_n$ with coefficients from the spatial function space $\mathscr{P}_h^j$; i.e.

$$\phi^h(\boldsymbol{x},t)=\sum_i\varphi_i^h(\boldsymbol{x})t^i,\quad \varphi_i^h\in\mathscr{P}_h^j, \tag{37}$$

where t^i is a monomial in $t\in I_n$ of order $i\in\mathbb{N}$. Denote by $\mathcal{S}_{_h}(Q_n;j,l)$, the space of admissible functions on the space-time domain Q_n of degree $j+l$ (that is, j in space and l in time):

$$\mathcal{S}_{_h}(Q_n;j,l)=\left\{\phi^h : \phi^h(\boldsymbol{x},t)=\sum_{i=0}^{l}\varphi_i^h(\boldsymbol{x})t^i,\ \varphi_i^h\in\mathscr{P}_h^j,\ (\boldsymbol{x},t)\in Q_n\right\}. \tag{38}$$

In fact, it is easy to observe that the space $\mathcal{S}_{_h}(Q_n;j,l)$ is generated by the tensor products of the basis elements of the spaces $\mathscr{P}_h^j$ and $P^l(I_n)$–the set of polynomials in time of degree at most j.

Remark:

1. The space-time mesh for Q_n is composed of cells with one element thickness in the time direction; and in each cell in the slab, time and space are orthogonal to each other, i.e. each cell is of the form $\Omega^e \times I_n$. Nevertheless, the formulation can be easily modified in terms of non-orthogonal space-time elements and with slabs composed of more than one element thickness in time direction as well.

2. The approach would readily accommodate the use of an adaptive mesh refinement procedures. In such cases, there may be cells with time direction thickness less than Δt_n embedded in slab Q_n. In this case, at each hanging node the solution must be constrained so that the hanging nodes will be condensed out.

Notations

Let φ and ψ be functions defined on space time domain slab Q_n. Some frequently used notations are

a) Spatial L^2 inner product

$$\langle \varphi, \psi \rangle := \int_\Omega \varphi\psi \ \mathrm{d}\Omega.$$

b) Space-time L^2 inner product

$$(\varphi, \psi)_{Q_n} := \int_{I_n} \langle \varphi, \psi \rangle \ \mathrm{d}t.$$

c) Space-time boundary integrals on $Z_n = \Gamma_{\mathbf{t}} \times I_n$ and $F_n = \Gamma_q \times I_n$

$$(\varphi, \psi)_{Z_n} = \int_{I_n} \int_{\Gamma_{\mathbf{t}}} \varphi\psi \ \mathrm{d}\Gamma \ \mathrm{d}t,$$
$$(\varphi, \psi)_{F_n} = \int_{I_n} \int_{\Gamma_q} \varphi\psi \ \mathrm{d}\Gamma \ \mathrm{d}t.$$

c) Right/left limit of a discontinuous function in time at t_n

$$\varphi(t_n^\pm) := \lim_{\varepsilon \to 0^\pm} \varphi(t_n + \varepsilon).$$

d) Temporal jump of a discontinuous function at t_n

$$[\![\varphi]\!]_n = \varphi(t_n^+) - \varphi(t_n^-).$$

4.1. Mechanical problem

In the mechanical phase the entropy is held fixed, so that the last equation of the left hand system in (29); that is the equation

$$\rho\Theta_0\dot{\eta} = \frac{\mathrm{d}}{\mathrm{d}t}[\rho c\vartheta + \rho\Theta_0 \mathbf{m} : \boldsymbol{\varepsilon}(\boldsymbol{u}) + S_0] = 0 \quad \text{ on } \quad \Omega \times [t_n, t_{n+1}) \tag{39}$$

is solved in closed form to obtain an *intermediate temperature* ϑ^I. This leads to an explicit formula for ϑ^I in terms of the state variables at time step t_n from the left and at time value $t \in (t_n,\ t_{n+1})$, that is,

$$\vartheta^I(t) = \vartheta(t_n^-) - \frac{\Theta_0}{c}\mathbf{m} : \boldsymbol{\varepsilon}(\boldsymbol{u}(t) - \boldsymbol{u}(t_n^-)) \qquad \text{for } \ t \in (t_n, t_{n+1}). \tag{40}$$

We substitute this result into the mechanical problem $(29)_1$ to obtain

$$\begin{aligned} \dot{\boldsymbol{u}} &= \boldsymbol{v}, \\ \rho\dot{\boldsymbol{v}} &= \mathrm{div}[\mathbb{C}_{ad}\boldsymbol{\varepsilon}(\boldsymbol{u})] + \boldsymbol{f}, \end{aligned} \tag{41}$$

where $\mathbb{C}_{ad} = \mathbb{C} + (\Theta_0/c)\mathbf{m} \otimes \mathbf{m}$, in the terminology used in [20], is referred to as *adiabatic elasticity tensor* and $\boldsymbol{f} = \rho\boldsymbol{b} - \mathbf{m}[\vartheta(t_n^-) + (\Theta_0/c)\mathbf{m} : \boldsymbol{u}(t_n^-)]$ and $\vartheta(t_n^-)$ and $\boldsymbol{u}(t_n^-)$ denote the temperature at the end of the previous space-time slab, Q_{n-1}. Note that the adiabatic elasticity tensor $\mathbb{C}_{ad}$ remains positive-definite and symmetric like $\mathbb{C}$.

On the current space-time slab, Q_n, we use same boundary conditions as given in (7) for the mechanical fields but the initial conditions, in this case, are the solution for $\boldsymbol{u}$ and $\boldsymbol{v}$ at the end of the previous slab; that is $\boldsymbol{u}(t_n^-)$ and $\boldsymbol{v}(t_n^-)$.

To define the T-DG FEM formulation of the mechanical problem (41), we first define the trial and weight function spaces for displacement $\boldsymbol{u}$ and velocity $\boldsymbol{v}$ vector fields as

$$\begin{aligned}
\mathcal{T}_h^u &= \left\{\boldsymbol{u}^h \in [\mathcal{S}_h(Q_n; j, l)]^d : \boldsymbol{u}^h = \bar{\boldsymbol{u}} \text{ on } \Gamma_{\boldsymbol{u}} \times I_n\right\}, \\
\mathcal{T}_h^v &= \left\{\boldsymbol{v}^h \in [\mathcal{S}_h(Q_n; j, l)]^d : \boldsymbol{v}^h = \dot{\bar{\boldsymbol{u}}} \text{ on } \Gamma_{\boldsymbol{u}} \times I_n\right\}, \\
\mathcal{W}_h^u &= \left\{\boldsymbol{w}^h \in [\mathcal{S}_h(Q_n; j, l)]^d : \boldsymbol{w}^h = \boldsymbol{0} \text{ on } \Gamma_{\boldsymbol{u}} \times I_n\right\}, \\
\mathcal{W}_h^v &= \left\{\boldsymbol{\varphi}^h \in [\mathcal{S}_h(Q_n; j, l)]^d : \boldsymbol{\varphi}^h = \boldsymbol{0} \text{ on } \Gamma_{\boldsymbol{u}} \times I_n\right\},
\end{aligned} \tag{42}$$

where $\mathcal{T}_h^u$ and $\mathcal{T}_h^v$, $\mathcal{W}_h^u$ and $\mathcal{W}_h^v$ are trial and weight function spaces for displacement and velocity vector fields respectively. The T-DG FEM is formulated as: find $\boldsymbol{U}^h = (\boldsymbol{u}^h, \boldsymbol{v}^h)^T \in \mathcal{T}_h^u \times \mathcal{T}_h^v$ such that for all $\boldsymbol{V}^h = (\boldsymbol{w}^h, \boldsymbol{\varphi}^h)^T \in \mathcal{W}_h^u \times \mathcal{W}_h^v$

$$A_n^M(\boldsymbol{U}^h, \boldsymbol{V}^h) = b_n^M(\boldsymbol{V}^h), \tag{43}$$

where

$$\begin{aligned}
A_n^M(\boldsymbol{U}^h, \boldsymbol{V}^h) &= (\dot{\boldsymbol{u}}^h, \boldsymbol{w}^h)_{Q_n} - (\boldsymbol{v}^h, \boldsymbol{w}^h)_{Q_n} + (\rho\dot{\boldsymbol{v}}^h, \boldsymbol{\varphi}^h)_{Q_n} + (\mathbb{C}_{ad}\boldsymbol{\varepsilon}(\boldsymbol{u}^h), \boldsymbol{\varepsilon}(\boldsymbol{\varphi}^h))_{Q_n} \\
&\quad + \langle \boldsymbol{u}^h(t_n^+), \boldsymbol{w}^h(t_n^+)\rangle + \langle \rho\boldsymbol{v}^h(t_n^+), \boldsymbol{\varphi}^h(t_n^+)\rangle \\
b_n^M(\boldsymbol{V}^h) &= (\bar{\mathbf{t}}, \boldsymbol{\varphi}^h)_{Z_n} + (\boldsymbol{f}, \boldsymbol{\varphi}^h)_{Q_n} + \langle \boldsymbol{u}^h(t_n^-), \boldsymbol{w}^h(t_n^+)\rangle + \langle \rho\boldsymbol{v}^h(t_n^-), \boldsymbol{\varphi}^h(t_n^+)\rangle.
\end{aligned} \tag{44}$$

Remark:

(1) The main difference between the DG formulation presented in (43) and that of [15] is the inner product used to enforce the continuity of displacement $(41)_1$ weakly. In our formulation the L^2-inner product in the pair $(\boldsymbol{u},\ \boldsymbol{v})$ is used to weakly enforce the mechanical problem while in [15] an energy-inner product is used.

(2) The formulation (43) is consistent in the sense of a time-stepping algorithm. This can be seen from the Euler-Lagrange form of (43) given by

$$\begin{aligned}
0 &= A_n^M(\boldsymbol{U}^h, \boldsymbol{V}^h) - b_n^M(\boldsymbol{V}^h) \\
&= (\dot{\boldsymbol{u}}^h - \boldsymbol{v}^h, \boldsymbol{w}^h)_{Q_n} + (\rho\dot{\boldsymbol{v}}^h - \operatorname{div}[\mathbb{C}_{ad}\boldsymbol{\varepsilon}(\boldsymbol{u})^h] - \boldsymbol{f}, \boldsymbol{\varphi}^h) && \text{(equation of motion)} \\
&\quad + \langle [\![\boldsymbol{u}^h]\!]_n, \boldsymbol{w}^h(t_n^+)\rangle && \text{(displacement continuity)} \\
&\quad + \langle [\![\rho\boldsymbol{v}^h]\!]_n, \boldsymbol{\varphi}^h(t_n^+)\rangle, && \text{(velocity continuity)}
\end{aligned} \tag{45}$$

that upon substitution of a sufficiently smooth solution pair $(\boldsymbol{u}, \boldsymbol{v})^T$ of the strong form (41) into (45), the weak forms of the jumps and the equation of motion vanish.

(3) The jump terms are used to improve the stability of the scheme without degrading the accuracy. As a result, the formalism can be readily extended to the non-linear case without eliminating the jump term from the displacement-velocity relation.

(4) One of the consequences of using the L^2-inner product is that a Dirchlet-type boundary condition may not be necessary to define the velocity trial and weight function spaces. Instead we can use

$$\mathcal{T}_h^v = \mathcal{W}_h^v = [\mathcal{S}_h(Q_n; j, l)]^d. \tag{46}$$

4.1.1. Stability: The mechanical algorithm

For the sake of simplicity, we assume a homogeneous source term $\boldsymbol{f} = \boldsymbol{0}$ and boundary conditions, i.e. $\bar{\mathbf{t}} = \boldsymbol{0}$ and $\bar{\boldsymbol{u}} = \boldsymbol{0}$. We claim that the formulation (43) renders an unconditionally stable time-stepping algorithm. That is to say:

$$\mathscr{E}_{M}(\boldsymbol{U}^h(t_{n+1}^-)) \leq \mathscr{E}_{M}(\boldsymbol{U}^h(t_n^-)) \quad \forall n = 0, 1, \cdots, N-1, \tag{47}$$

where $\mathscr{E}_{M}(\boldsymbol{U}(t))$ is the total mechanical energy of $\boldsymbol{U} = (\boldsymbol{u}, \boldsymbol{v})^T$ at time t, given by

$$\mathscr{E}_{M}(\boldsymbol{U}(t)) = \frac{1}{2}\int_{\Omega} \left[\boldsymbol{\varepsilon}(\boldsymbol{u}(t)) : \mathbb{C}_{ad}\boldsymbol{\varepsilon}(\boldsymbol{u}(t)) + \rho \boldsymbol{v}(t)\cdot\boldsymbol{v}(t)\right] \mathrm{d}\Omega. \tag{48}$$

For the analysis we use elliptic and L^2 interpolation operators $\boldsymbol{\pi} : [H_{\Gamma_u}(\Omega)]^d \to \mathcal{W}_h^u(t)$ and $\hat{\boldsymbol{\pi}} : [L^2(\Omega)]^d \to \mathcal{W}_h^u(t)$ respectively defined as: for $\boldsymbol{u} \in [H_{\Gamma_u}(\Omega)]^d$ and $\boldsymbol{w} \in [L^2(\Omega)]^d$

$$\begin{aligned} \langle \mathbf{C}_{ad}\boldsymbol{\varepsilon}(\boldsymbol{\pi}\boldsymbol{u}), \boldsymbol{\varepsilon}(\boldsymbol{\varphi}^h)\rangle &= \langle \mathbf{C}_{ad}\boldsymbol{\varepsilon}(\boldsymbol{u}), \boldsymbol{\varepsilon}(\boldsymbol{\varphi}^h)\rangle, \qquad && \forall \boldsymbol{\varphi}^h \in \mathcal{W}_h^u(t), \\ \langle \hat{\boldsymbol{\pi}}\boldsymbol{w}, \boldsymbol{\psi}^h\rangle &= \langle \boldsymbol{w}, \boldsymbol{\psi}^h\rangle, && \forall \boldsymbol{\psi}^h \in \mathcal{W}_h^u(t), \end{aligned} \tag{49}$$

where $\mathcal{W}_h^u(t)$ refers to the space of functions in $\mathcal{W}_h^u$ at a fixed but arbitrary $t \in I_n$. We also use the fact that [26]

$$\mathrm{div}[\mathbb{C}_{ad}\boldsymbol{\varepsilon}(\boldsymbol{\pi}\boldsymbol{u})] = \hat{\boldsymbol{\pi}}\mathrm{div}[\mathbb{C}_{ad}\boldsymbol{\varepsilon}(\boldsymbol{u})]. \tag{50}$$

Now, given the solution $\boldsymbol{U}^h(t_n^-) = (\boldsymbol{u}^h(t_n^-), \boldsymbol{v}^h(t_n^-))^T$ of (43) at the end of the previous space-time slab, Q_{n-1}, and let $\boldsymbol{U}^h(t) = (\boldsymbol{u}^h(t), \boldsymbol{v}^h(t))^T$ be the solution of (43) in the current space-time slab, Q_n. Replace $\boldsymbol{V}^h = (\hat{\boldsymbol{\pi}}\mathrm{div}[\mathbb{C}_{ad}\boldsymbol{\varepsilon}(\boldsymbol{u}^h)], \boldsymbol{0})^T$ in (43) to obtain

$$\begin{aligned} 0 = &(\dot{\boldsymbol{u}}^h, \hat{\boldsymbol{\pi}}\mathrm{div}[\mathbb{C}_{ad}\boldsymbol{\varepsilon}(\boldsymbol{u}^h)])_{Q_n} - (\boldsymbol{v}^h, \hat{\boldsymbol{\pi}}\mathrm{div}[\mathbb{C}_{ad}\boldsymbol{\varepsilon}(\boldsymbol{u}^h)])_{Q_n} \\ &+ \langle [\![\boldsymbol{u}^h]\!]_n, \hat{\boldsymbol{\pi}}\mathrm{div}[\mathbb{C}_{ad}\boldsymbol{\varepsilon}(\boldsymbol{u}^h(t_n^+))]\rangle. \end{aligned} \tag{51}$$

Applying (50) in (51) and the definition of the projection operator $\boldsymbol{\pi}$ and using integration by parts (note the homogeneous boundary conditions) leads to

$$\begin{aligned} 0 = &(\boldsymbol{\varepsilon}(\dot{\boldsymbol{u}}^h), \mathbb{C}_{ad}\boldsymbol{\varepsilon}(\boldsymbol{u}^h))_{Q_n} - (\boldsymbol{\varepsilon}(\boldsymbol{v}^h), \mathbb{C}_{ad}\boldsymbol{\varepsilon}(\boldsymbol{u}^h))_{Q_n} \\ &+ \langle [\![\boldsymbol{\varepsilon}(\boldsymbol{u}^h)]\!]_n, \mathbb{C}_{ad}\boldsymbol{\varepsilon}(\boldsymbol{u}^h(t_n^+))\rangle. \end{aligned} \tag{52}$$

Again substituting $\boldsymbol{V}^h = (\boldsymbol{0}, \boldsymbol{v}^h)^T$ into (43) yields

$$0 = (\rho\dot{\boldsymbol{v}}^h, \boldsymbol{v}^h)_{Q_n} + (\mathbb{C}_{ad}\boldsymbol{\varepsilon}(\boldsymbol{u}^h), \boldsymbol{\varepsilon}(v))_{Q_n} + \langle [\![\rho\boldsymbol{v}^h]\!]_n, \boldsymbol{v}^h(t_n^+)\rangle. \tag{53}$$

Adding the equations (52) and (53) we obtain

$$(\boldsymbol{\varepsilon}(\dot{\boldsymbol{u}}^h), \mathbb{C}_{ad}\boldsymbol{\varepsilon}(\boldsymbol{u}^h))_{Q_n} + (\rho\dot{\boldsymbol{v}}^h, \boldsymbol{v}^h)_{Q_n} + \langle [\![\boldsymbol{\varepsilon}(\boldsymbol{u}^h)]\!]_n, \mathbb{C}_{ad}\boldsymbol{\varepsilon}(\boldsymbol{u}^h(t_n^+))\rangle + \langle [\![\rho\boldsymbol{v}^h]\!]_n, \boldsymbol{v}^h(t_n^+)\rangle = 0. \tag{54}$$

Taking the time derivative out of the space integral, (54) becomes

$$\begin{aligned} &\frac{1}{2}(\boldsymbol{\varepsilon}(\boldsymbol{u}^h(t_{n+1}^-)), \mathbb{C}_{ad}\boldsymbol{\varepsilon}(\boldsymbol{u}^h(t_{n+1}^-)))_{Q_n} + \frac{1}{2}(\rho\boldsymbol{v}^h(t_{n+1}^-), \boldsymbol{v}^h(t_{n+1}^-))_{Q_n} \\ &- \frac{1}{2}(\boldsymbol{\varepsilon}(\boldsymbol{u}^h(t_n^+)), \mathbb{C}_{ad}\boldsymbol{\varepsilon}(\boldsymbol{u}^h(t_n^+)))_{Q_n} - \frac{1}{2}(\rho\boldsymbol{v}^h(t_n^+), \boldsymbol{v}^h(t_n^+))_{Q_n} \\ &+ \langle [\![\boldsymbol{\varepsilon}(\boldsymbol{u}^h)]\!]_n, \mathbb{C}_{ad}\boldsymbol{\varepsilon}(\boldsymbol{u}^h(t_n^+))\rangle + \langle [\![\rho\boldsymbol{v}^h]\!]_n, \boldsymbol{v}^h(t_n^+)\rangle = 0. \end{aligned} \tag{55}$$

After some algebraic manipulation we obtain

$$\mathscr{E}_{M}(\boldsymbol{U}^h(t_{n+1}^-)) + \mathscr{E}_{M}([\![\boldsymbol{U}^h]\!]_n) = \mathscr{E}_{M}(\boldsymbol{U}^h(t_n^-)). \tag{56}$$

Since $\mathscr{E}_{M}([\![\boldsymbol{U}^h]\!]_n)$ is non-negative the energy equation (56) leads to the estimate (47) that renders the scheme for the mechanical phase (43) unconditionally stable. In fact, the total numerical dissipation added is precisely equal to

$$\sum_{n=0}^{N-1} \mathscr{E}_{M}([\![\boldsymbol{U}^h]\!]_n).$$

Remark:

The use of projection operators in (49) and (51) reveals an important point, that is, the current T-DG formulation can be converted into the one given in [15].

4.2. Thermal problem

The solution $\boldsymbol{U}^h(t_{n+1}^-)$ of the mechanical phase is known at the end of the current space-time slab. The objective, in the present phase, is to solve for the thermal states $\boldsymbol{\Pi}(t) = (\alpha(t), \vartheta(t))^T$, $t \in I_n$. Hence, the global solution at the end of the current slab will be $(\boldsymbol{U}^h(t_{n+1}^-), \boldsymbol{\Pi}^h(t_{n+1}^-))$.

The operator-splitting is performed based on the state vector $\boldsymbol{\Sigma} = (\boldsymbol{u}, \boldsymbol{v}, \alpha, \eta)^T$. As a result, we enforce the problem in the thermal phase using the conservation form

$$\begin{aligned} \dot{\alpha} &= \Theta, \\ \rho\Theta_0\dot{\eta} &= \operatorname{div}[\mathbf{k}_2\nabla\alpha + \mathbf{k}_3\nabla\Theta] + \rho r. \end{aligned} \tag{57}$$

Here, recall that the entropy density η is obtained from the relation $\rho\eta = \dfrac{c\rho}{\Theta_0}\vartheta + \mathbf{m} : \boldsymbol{\varepsilon}(\boldsymbol{u}) + S_0$.

In the thermal phase, the displacement $\boldsymbol{u}$ and the velocity $\boldsymbol{v}$ are fixed at the corresponding values at the end of the current slab in the mechanical phase; that is,

$$\boldsymbol{u}_T(t) = \boldsymbol{u}_M(t_{n+1}^-), \quad \boldsymbol{v}_T(t) = \boldsymbol{v}_M(t_{n+1}^-), \qquad t \in I_n, \tag{58}$$

where the subscripts T and M represents the values of the fields in the thermal and mechanical phases, respectively. Thus, the time derivative of the terms $\mathbf{m} : \boldsymbol{\varepsilon}(\boldsymbol{u}) + S_0$ vanishes, and consequently the left hand side of equation $(57)_2$ becomes

$$\rho\Theta_0\dot{\eta} = \rho c\dot{\vartheta}. \tag{59}$$

In addition, the jump in the entropy, in this case, reads as

$$\begin{aligned} [\![\rho\Theta_0\eta]\!]_n &= \rho\Theta_0\eta(t_n^+) - \rho\Theta_0\eta(t_n^-) \\ &= \left[\rho c\vartheta(t_n^+) + \rho\Theta_0\mathbf{m} : \boldsymbol{\varepsilon}(\boldsymbol{u}_M(t_{n+1}^-)) + S_0\right] - \left[\rho c\vartheta(t_n^-) + \rho\Theta_0\mathbf{m} : \boldsymbol{\varepsilon}(\boldsymbol{u}(t_n^-)) + S_0\right] \\ &= [\![\rho c\vartheta]\!]_n + \rho\Theta_0\mathbf{m} : [\boldsymbol{\varepsilon}(\boldsymbol{u}_M(t_{n+1}^-)) - \boldsymbol{\varepsilon}(\boldsymbol{u}(t_n^-))]. \end{aligned} \tag{60}$$

It should not cause any confusion if we drop the superscript M in the equation (60) so that the jump term can be written as

$$[\![\rho\Theta_0\eta]\!]_n = [\![\rho c\vartheta]\!]_n + \rho\Theta_0\mathbf{m} : [\boldsymbol{\varepsilon}(\boldsymbol{u}(t_{n+1}^-)) - \boldsymbol{\varepsilon}(\boldsymbol{u}(t_n^-))]. \tag{61}$$

To define the T-DG formulation for the thermal phase we first define the thermal displacement and temperature trial and weight function spaces $\mathcal{T}_h^{\alpha}$, $\mathcal{T}_h^{\vartheta}$ and $\mathcal{W}_h^{\alpha}$, $\mathcal{W}_h^{\vartheta}$ respectively based on $\mathcal{S}_h(Q_n; j, l)$ and the boundary condition requirements.

$$\begin{aligned} \mathcal{T}_h^{\alpha} &= \left\{\alpha^h \in \mathcal{S}_h(Q_n; j, l) : \dot{\alpha}^h = \bar{\Theta} \text{ on } \Gamma_\alpha \times I_n\right\}, \\ \mathcal{T}_h^{\vartheta} &= \left\{\vartheta^h \in \mathcal{S}_h(Q_n; j, l) : \Theta^h = \bar{\Theta} \text{ on } \Gamma_\alpha \times I_n\right\}, \\ \mathcal{W}_h^{\alpha} &= \left\{\beta^h \in \mathcal{S}_h(Q_n; j, l) : \beta^h = 0 \text{ on } \Gamma_\alpha \times I_n\right\}, \\ \mathcal{W}_h^{\vartheta} &= \left\{\sigma^h \in \mathcal{S}_h(Q_n; j, l) : \sigma^h = 0 \text{ on } \Gamma_\alpha \times I_n\right\}. \end{aligned} \tag{62}$$

Formally, the T-DG FEM formulation of the thermal phase on the domain Q_n is defined as: find $\boldsymbol{\Pi}^h = (\alpha, \vartheta)^T \in \mathcal{T}_h^{\alpha} \times \mathcal{T}_h^{\vartheta}$ such that for each $\boldsymbol{\Lambda}^h = (\beta^h, \sigma^h)^T \in \mathcal{W}_h^{\alpha} \times \mathcal{W}_h^{\vartheta}$

$$A_n^T(\boldsymbol{\Pi}^h, \boldsymbol{\Lambda}^h) = b_n^T(\boldsymbol{\Lambda}^h), \tag{63}$$

where

$$
\begin{aligned}
A_n^T(\mathbf{\Pi}^h, \mathbf{\Lambda}^h) &= (\dot{\alpha}^h, \beta^h)_{Q_n} - (\Theta^h, \beta^h)_{Q_n} + (\rho c \dot{\vartheta}^h, \sigma^h)_{Q_n} + ([\mathbf{k}_2 \nabla \alpha^h + \mathbf{k}_3 \nabla \theta^h], \nabla \sigma^h)_{Q_n}, \\
&\quad + \langle \alpha^h(t_n^+), \beta^h(t_n^+) \rangle + \langle \rho c \vartheta^h(t_n^+), \sigma^h(t_n^+) \rangle \\
b_n^T(\mathbf{\Lambda}^h) &= \langle \alpha^h(t_n^-), \beta^h(t_n^+) \rangle + \langle \rho c \vartheta^h(t_n^-), \sigma^h(t_n^+) \rangle + \langle \rho \Theta_0 [\boldsymbol{\varepsilon}(\boldsymbol{u}(t_n^-)) - \boldsymbol{\varepsilon}(\boldsymbol{u}(t_{n+1}^-))], \sigma^h(t_n^-) \rangle \\
&\quad + (\bar{h}, \sigma^h)_{F_n} + (\rho r, \sigma^h)_{Q_n}.
\end{aligned}
\tag{64}
$$

The relation between the DG formulation (63) and the point-wise form (57) is apparent from the Euler-Lagrange form

$$
\begin{aligned}
0 = {} & A_n^T(\mathbf{\Pi}^h, \mathbf{\Lambda}^h) - b_n^T(\mathbf{\Lambda}^h) \\
& + (\dot{\alpha} - \Theta^h, \beta^h)_{Q_n} \\
& + (\rho \Theta_0 \dot{\eta} + \operatorname{div}[\mathbf{k}_2 \nabla \alpha^h + \mathbf{k}_3 \nabla \theta^h] + \rho r, \sigma^h)_{Q_n} && \text{(Equation of motion)} \\
& + \langle [\![\alpha^h]\!]_n, \beta^h(t_n^+) \rangle && (\alpha\text{-continuity}) \\
& + \langle [\![\rho c \vartheta^h]\!]_n, \sigma^h(t_n^+) \rangle, && (\vartheta\text{-continuity})
\end{aligned}
\tag{65}
$$

which reveals that a sufficiently smooth solution of the strong problem (57) also satisfies (63), and vice versa, while the jump terms are vanished at the smooth solution. This also proves the consistency of the T-DG scheme of the thermal problem.

The unconditionally stability of the scheme (63) can also be shown along the same line of argument used for the mechanical case.

Remark:

- Again, the use of the L^2-inner product to enforce the thermal problem allows one to omit the boundary restriction when we define the thermal displacement trial and weight function space. i.e.

$$
\mathcal{T}_h^\alpha := \mathcal{S}_h(Q_n; j, l) =: \mathcal{W}_h^\alpha. \tag{66}
$$

  This is a very important observation in terms of practical implementation.

As we have seen from Section 3 that consistent and stable sub-algorithms render a consistent and stable global algorithm in the sense of time-stepping algorithms based on operator-splitting. Both the mechanical and the thermal phase algorithms are shown to be consistent and unconditionally stable. Therefore, the algorithm for the global problem based on Lie-Trotter-Kato product formula is consistent and unconditionally stable. Moreover, the convergence of the global scheme follows from the well known result stated below.

Theorem 1 (Lax Equivalence Theorem). *For **consistent** numerical approximations, **stability** is equivalent to **convergence**.*

5. Numerical results

In this section, we present a range of numerical results for type II and III problems of non-classical thermoelasticity. We start by comparing convergence of the proposed splitting scheme against a monolithic approach in which all the governing equations are discretized simultaneously using the time-DG finite element method. For this, a 1-D problem of non-dimensional form is considered. The result shows excellent agreement between the monolithic and the splitting scheme. Then we present various results in 1-D and 2-D. The examples in this case are designed to illustrate two key features of the time-DG scheme: (i) its performance in solving problems that involves the propagation of sharp gradients without creating spurious oscillations; and (ii) its capability in capturing the unique aspects of non-classical theory, for example, propagation of thermal wave and its complex response due to the coupling of elasticity problem.

The family of problems considered in this section are organized as follows. To analyse the rate of convergence and capability of the proposed scheme, a non-dimensional form of a 1-D non-classical thermoelastic problem is presented in Section 5.1. The performance of the splitting algorithm is examined in Section 5.2 for an initial temperature pulse propagation in a two dimensional square plate under plane strain condition. Finally, in Section 5.3, a quasi-static expansion of a thick walled, infinitely long cylinder in plane strain condition is presented, which is modelled using type I and type III thermoelasticity and the remarkable difference of thermal responses between the two models are also analysed.

All simulations were performed on an Intel Core i7-4700MQ processor of 8 cores each at 2.4 GHz and memory capacity of 8 GB. The efficiency of the monolithic and splitting algorithms was compared using a serial computation on a single core.

The 1-D problems were solved using a Matlab [28] time-discontinuous finite element programs for both the monolithic and splitting approaches. Routines for computing the element contributions on rectangular space-time elements were constructed analytically in Mathematica [29] and then exported to Matlab. All computations were performed on uniform space-time meshes. As a result, element contributions were computed automatically from a typical space-time cell. MATLAB's direct solver is used for all computations in the 1-D case.

The 2-D problems were solved using a Mathematica-based time-discontinuous Galerkin finite element code developed by the authors which utilizes AceGEN/FEM library [30]. AceGEN/FEM is a general finite element library for Mathematica which combines symbolic and numeric approaches. AceFEM uses the parallelized direct solver PARDISO [31, 32].

5.1. Non-dimensional 1-D GNT

The non-dimensional form of 1-D GNT problem given in (1) is

$$\begin{aligned}
&\partial_\tau \bar{u} = \bar{v},\\
&\partial_\tau \bar{v} = \partial_\xi[\varepsilon_1 \partial_\xi \bar{u} - \bar{\vartheta}] + \bar{b},\\
&\partial_\tau \bar{\alpha} = \bar{\vartheta},\\
&\partial_\tau \bar{\vartheta} = \partial_\xi[\partial_\xi \alpha + k\partial_\xi \bar{\vartheta}] - \varepsilon_2 \partial_\xi \bar{v} + \bar{s},
\end{aligned} \tag{67}$$

with the dimensionless parameters

$$\varepsilon_1 = (\frac{v_f}{v_s})^2, \qquad \varepsilon_2 = \frac{\Theta_0 m^2 E}{\rho c}, \quad \text{and} \quad k = \frac{k_3}{\sqrt{\rho c}}, \tag{68}$$

where ε_1 denotes the square of the ratio of uncoupled velocities of the mechanical wave (or first sound) and thermal wave (or second sound), ε_2 denotes the strength of the thermomechanical coupling, k represents the non-dimensional classical heat conductivity. The speed of first sound v_f is the speed of sound in the medium, that is

$$v_f = \sqrt{\frac{E}{\rho}}, \tag{69}$$

where E denotes the Young's modulus of the medium, while that of the second sound v_s is a characteristic feature of the theory of non-classical heat conduction by Green and Naghdi that represents the speed in which a thermal disturbance travels through the medium:

$$v_s = \sqrt{\frac{k_2}{\rho c}}. \tag{70}$$

The non-dimensionless variables are given by

$$\xi = x_c^{-1} x, \quad \tau = t_c^{-1} t, \quad \bar{u} = u_c^{-1} u, \quad \bar{v} = \frac{t_c}{u_c} v, \quad \bar{\alpha} = \alpha_c^{-1} \alpha, \quad \bar{\vartheta} = \frac{t_c}{\alpha_c} \vartheta, \tag{71}$$

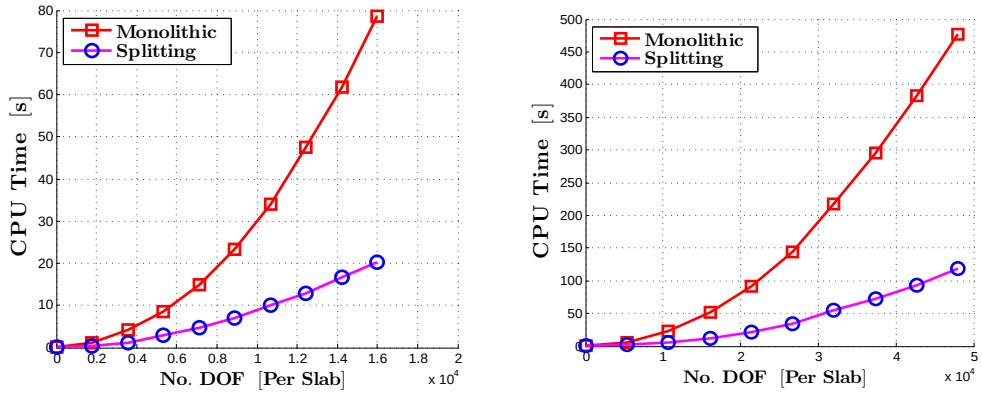

(a) Q1 (b) Q2

Figure 1: Comparison of efficiency of the monolithic and splitting algorithms in Q1 and Q2 cases. CPU time is measured using a serial computation on a single core.

where x_c, t_c, u_c, α_c are characteristic quantities having the same dimension as x, t, u, α respectively that can be chosen according to the relations

$$\frac{x_c}{t_c} = v_s, \quad \frac{u_c}{\alpha_c} = \frac{m v_f}{\rho}. \tag{72}$$

From the above equations we can observe that there are infinitely many ways of choosing the characteristics constants without changing the form of the system (67).

The nondimensional energy counterpart of (17), also referred to as the H^1 norm, is given by

$$[\mathcal{E}(\bar{\boldsymbol{\chi}})]^2 = \int_0^{\bar{L}} \left[\varepsilon_1 [\partial_\xi \bar{u}]^2 + \bar{v}^2 + \frac{1}{\varepsilon_2} [\partial_\xi \bar{\alpha}]^2 + \frac{1}{\varepsilon_2} \bar{\vartheta}^2 \right] \mathrm{d}\xi, \tag{73}$$

and the L^2-norm

$$\|\bar{\boldsymbol{\chi}}\|^2 = \int_0^{\bar{L}} \left[\bar{u}^2 + \bar{v}^2 + \bar{\alpha}^2 + \bar{\vartheta}^2 \right] \mathrm{d}\xi, \tag{74}$$

where $\bar{\boldsymbol{\chi}} = (\bar{u}, \bar{v}, \bar{\alpha}, \bar{\vartheta})^T$ is the state vector at a given time.

5.1.1. Convergence

For the purpose of the convergence analysis an exact solution to problem (67) is obtained in such a way that source terms $\bar{b}$ and $\bar{s}$ are suitably prescribed such that a given state vector $\bar{\boldsymbol{\chi}} = (\bar{u}, \bar{\alpha}, \bar{\alpha}, \bar{\vartheta})^T$ is an exact solution [18]. To this end let the source terms be

$$\begin{aligned} \bar{b} &= \frac{\pi^2}{4} \left[(\varepsilon_1 - 1) \sin(\pi\xi) \sin(\pi\tau) + \cos(\pi\xi) \cos(\pi\tau) \right], \\ \bar{s} &= \frac{\pi^2}{4} \left[k\pi \sin(\pi\xi) \cos(\pi t) + \varepsilon_2 \cos(\pi\xi) \cos(\pi\tau) \right], \end{aligned} \tag{75}$$

so that the exact solutions are

$$\begin{aligned} \bar{u}(\xi,\tau) = \bar{\alpha} &= \frac{1}{4} \sin(\pi\xi) \sin(\pi\tau), \\ \bar{v}(\xi,\tau) = \bar{\vartheta} &= \frac{\pi}{4} \sin(\pi\xi) \cos(\pi\tau), \end{aligned} \tag{76}$$

defined on the space-time domain $(\xi, \tau) \in [0, \bar{L}] \times [0, \bar{T}]$. For convergence analysis the values of the non-dimensional parameters are taken as $\varepsilon_1 = 4$, $\varepsilon_2 = 0.2$, $k = 0$. Such set of values represents a strongly coupled

problem of two purely hyperbolic systems (type II thermoelasticity). The space-time domain corresponds to $\bar{L} = 1$ and $\bar{T} = 0.25$. Simulations were performed using both bilinear Q1 and biquadratic Q2 finite elements in each space-time slab with each element having an aspect ratio of one (i.e. $h = \Delta\xi = \Delta\tau$).

To compare the convergence rates of the monolithic and splitting schemes, we evaluate the L^2 and H^1 norms (spatial integrals over $[0,\ \bar{L}]$), as given in equations (73) and (74), respectively, of the error $\boldsymbol{e} = \boldsymbol{\chi}_{\text{ex}}(\bar{T}) - \boldsymbol{\chi}^h(\bar{T})$, where $\boldsymbol{\chi}_{\text{ex}}$ denotes the exact solution (76) and $\boldsymbol{\chi}^h$ the numerical solution corresponding to the source terms (75). Fig. 2 (a) & (b) report the *spatial convergence* results of the monolithic and operator-splitting approaches with Q1 and Q2 space-time finite element interpolations, respectively. Fig. 2 (a) shows a superlinear order of convergence of the Q1 splitting scheme, whereas the monolithic scheme is shown to have convergence of second-order. In contrast, Fig. 2 (b) shows that the convergence of the splitting scheme is degraded to just first-order with Q2, while the monolithic scheme shows more than cubic order of convergence.

While Fig. 2 (c) & (d) present the result of *temporal convergence* results of the two approaches with errors of the approximate solutions computed at the mid-point, $\xi = \bar{L}/2$, and $\tau = \bar{T}$ using the ℓ_2 vector norm. Almost the same convergence behaviour is also demonstrated temporally as was shown spatially. In this case, it is shown that splitting scheme performs better in Q1 than in Q2. Remarkably, the temporal convergence of the monolithic scheme is increased by more than 100 % from Q1 and Q2. As it is expected, the first-order operator-splitting scheme performs poorly in Q2.

To compare efficiency of the two algorithms, the respective codes are organized in such a way that computations of the element stiffness matrices and right hand-side vectors are based on essentially the same optimized routines. MATLAB's direct solver were used in both schemes. The only major factor that determines the efficiency of the codes of the two schemes is the time spent in solving the linear systems at each step. For this, Fig. 1 (a) & (b) are summarizing the time spent by each of the approaches as the space-time domain is uniformly refined. The horizontal axes show the total number of degree-of-freedoms per slab while the vertical axis represents the corresponding CPU times that the cpu spent in running each algorithms. As it shown from the figures, the times in both Q1 and Q2 grows in the same fashion. Considering the difference in convergence rates between the monolithic and splitting schemes in low order approximations such as Q1, the latter approach might be advantageous in terms of efficiency. However, this is not the case for the Q2 approximation as it is evident from the gain in the case of the monolithic approach and the loss in the case of the splitting scheme as we move from lower- to higher-order schemes. However, as it was discussed in Section 3 a second-order algorithm $(28)_1$ can be constructed. The construction and analysis of such higher-order operator-splitting algorithms are out of the scope the present paper and will be dealt in the future work.

5.1.2. Laser pulse propagation

Consider a one-dimensional bar occupying the interval $\xi \in [0, 1]$, heated by a pulsing laser applied at the left end having the form similar to the one considered in [27] for non-Fourier heat conduction problem:

$$\bar{s}(\xi, \tau) = \frac{1}{D\tau_{_p}} \exp\left[\left(\frac{\xi}{D}\right)^2 - \left(\frac{\tau}{\tau_{_p}}\right)^2\right], \tag{77}$$

where D is the depth of the pulse, and $\tau_{_p}$ is characteristic duration of the pulse. The bar is clamped at both ends at all times and with homogeneous initial conditions. We consider a situation in which a highly localized thermal pulse both in space and time described by the constants $\tau_{_p} = 0.01$ and $D = 0.02$ is applied at the left end of the bar. The parameters considered here are $\varepsilon_1 = 9$, which represents $3:1$ ratio of *uncoupled* speeds of first sound to second sound, and $\varepsilon_2 = 1$ accounting for a strongly coupled system. Bilinear elements Q1 are used in each space-time slab with mesh dimension $\Delta\xi = \Delta\tau = h$. The simulations are carried out over the period of $\bar{T} = 1$ unit of non-dimensional time. The mesh parameter $h = 0.001$ is chosen such that the width of the pulse is greater than the mesh size. In other words, the mesh is chosen so that the thin laser pulse can be described accurately by the bilinear finite elements.

Fig. 3 (a) & (b) show the propagation, in space and time, of the thermal disturbance caused by the pulsing laser heat source applied at the left end of the bar, computed using the monolithic and the splitting

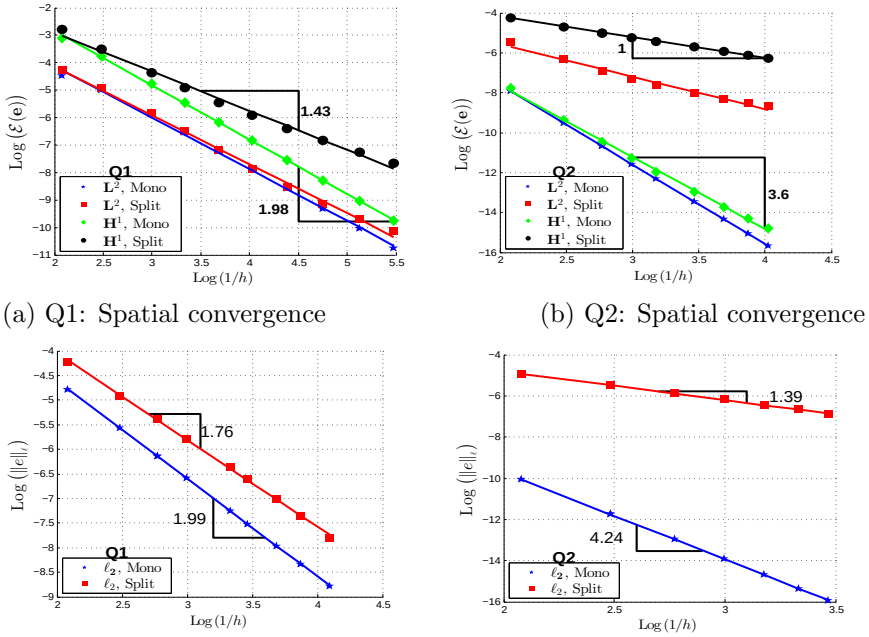

(a) Q1: Spatial convergence

(b) Q2: Spatial convergence

(c) Q1: Temporal convergence

(d) Q2: Temporal convergence

Figure 2: Type II thermo-mechanical problem: Rate of convergence using monolithic and splitting approaches where the error norms in (a) and (b) are computed at $\tau = 0.25$ over the whole spatial domain, while the ℓ_2-errors are evaluated at $\tau = \bar{T}/4$ and $\xi = \bar{L}/2$.

schemes, respectively. As can be seen from the figures, immediately after the pulse is applied, two thermal waves with different amplitude and speed start to emerge. The larger and the slower wave is the one which is driven by the thermal equations, while the smaller and the faster one is induced by the mechanical equations through the coupling. The larger thermal wave travels with a speed slightly less than that of second sound; whereas, the smaller thermal wave is travelling with a speed slightly greater than that of first sound. For this reason, it appears that the larger wave traverses the bar once, while the smaller traverses it more than three times. Note that the ratio of uncoupled speed of first to second sound is exactly $3:1$.

There are two features which show the strength of the thermomechanical coupling: the first one is that the ratio of the speeds of the two thermal waves is noticeably different from what is expected in the uncoupled case, and the other is that the coupling is strong enough to induce considerably large stress wave which in turn induces the faster thermal wave.

Moreover, this problem represents a strongly coupled problem of two second-order hyperbolic problems involving propagation of sharp gradients. Such a problem is typically very difficult to approximate using the standard semi-discrete approach (MoL) unless some kind of stabilization term (or an artificial viscosity) is added, which is basically equivalent to changing the system from non-dissipative to dissipative, or a very fine mesh is used together with a very small time-step, which is undesirable from a computational cost point of view.

What is remarkable about the current scheme is that it resolves the propagation of high gradients accurately while the amplitude of the thermal waves appear to be constant showing that the very small numerical dissipation is enough to damp out any numerical oscillation. The two approximate solution profiles Fig. 3 (a) and (b) are nearly identical. The agreement demonstrates that the splitting scheme maintains the accuracy of the monolithic scheme while the efficiency is considerably improved by the splitting scheme since two smaller systems are solved at each space-time slab. The result obtained here can be qualitatively compared to the one obtained in [21].

As shown from Fig. 4, other than some small numerical instabilities when the waves interact either with

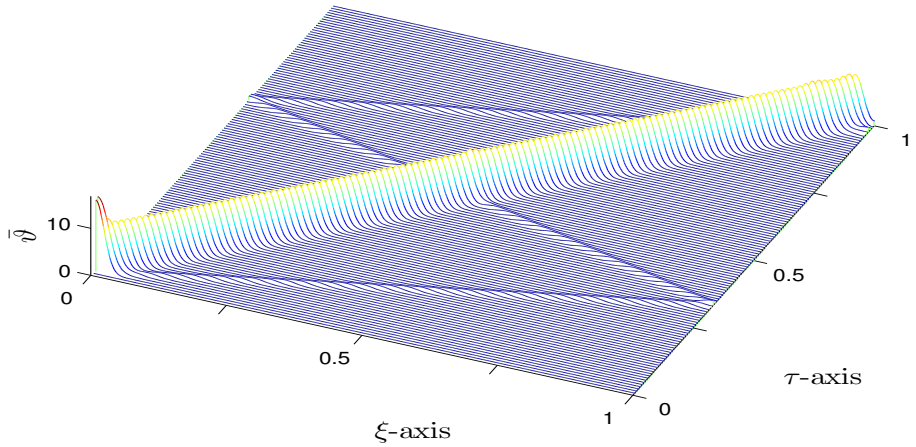

(a) Monolithic

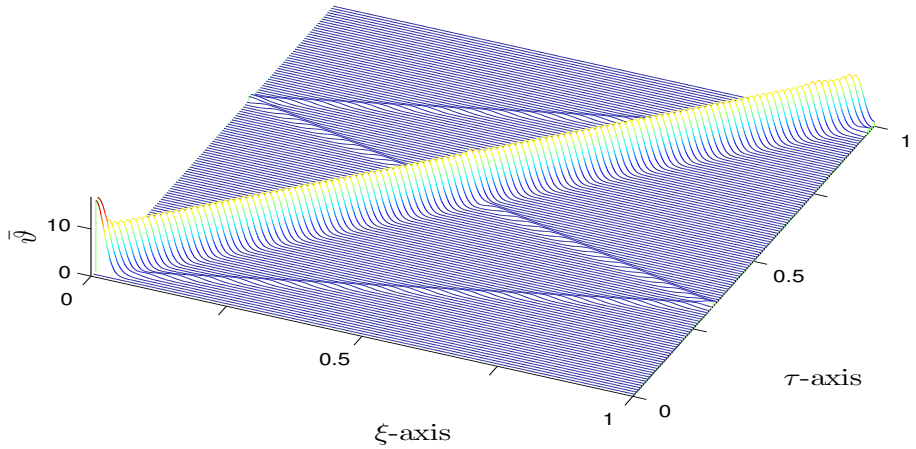

(b) Splitting

Figure 3: Propagation of laser pulse in type II thermoelasticity: temperature profile of the rod over the time period with $\varepsilon_1 = 9$, $\varepsilon_2 = 0.5$, $k = 0$ and $\Delta\xi = \Delta\tau = 0.001$.

the boundary or each other, the energy gained computed using the H^1-norm, remains essentially constant after the pulse is applied. This phenomenon is characteristic feature of type II thermoelasticity which is proved in Section 2.2. While the L^2-norm shows more profound variation than the energy-norm immediately after the pulse is applied and when the two waves interact with each other but it shows no change when the waves interact with the boundary. These observations suggest that the numerical instability that arises from the the interaction of waves with the boundaries may come from errors in the gradient of the approximate solution states.

Fig. 5 (a) and (b) show the temperature profiles for $k = 0.1$, which correspond to Type III thermoelasticity, approximated using the monolithic and splitting schemes, respectively. This case is characterized by dissipation of energy while a wave scenario is still evident. The thermal wave driven by the temperature equations is damped out quickly, whereas, the mechanically induced thermal wave remains localized for almost the entire duration and is travelling with speed nearly equal to the speed of the first sound.

5.2. Two dimensional problem: Initial heat pulse propagation

In this problem, we consider a non-dimensional form of type III problem of initial thermal pulse propagation in a square plate occupying the region $\Omega = [-1, 1] \times [-1, 1]$ under a plane strain assumption. A similar problem is solved in [21]. The boundary of the specimen is mechanically clamped and fixed at the reference temperature $\Theta_0 = 1$ (i.e. the temperature of the ambient space). Initially, it is at rest but a temperature pulse is initialized at the center of the plate. i.e. the initial condition for the relative temperature ϑ is

$$\vartheta(\boldsymbol{x}, 0) = A \exp\left[\frac{\boldsymbol{x} \cdot \boldsymbol{x}}{D}\right], \tag{78}$$

where D, as in the previous example in Section 5.1.2, is a constant characterizing the width of the initial temperature pulse and A is the amplitude. The material parameter used in the simulation are scaled according to the specifications summarized in Table 1. The T-DG finite element mesh consists of 8 node isoparametric cubes with one element thickness $\Delta t = 0.01$ in the time direction and 100×100 spatial elements per each slab are used to sufficiently describe the initial thermal pulse propagation.

Fig. 6 shows snapshots of propagation of an initial temperature pulse with $D = 100$ and $A = 4$ at times $t = 0$, $t = 0.2$, $t = 0.3$, and $t = 0.4$. The initial pulse may be thought of as a thermal configuration just after an intense and highly localized laser heat source is applied at the center. The temperature profile gradually widens and a smaller but faster mechanically driven wave emerges, while the the second sound wave is driven by the temperature equations moves with a slower speed. In this case, the classical conductivity parameter κ_2 gives additional stability but it is not so high to smear out the two wave phenomena.

5.3. Quasi-static case: Expansion of a thick walled cylinder

This problem deals with the quasi-static thermo-mechanical interaction in a thick walled cylinder as it expands as a result of an inner wall Dirichlet-type boundary condition, in the plane strain case. The material considered is isotropic both thermally and mechanically. The thermal variation is purely the result of mechanical changes (the expansion of the cylinder) unlike in the previous examples (Sections 5.1.2 and 5.2) in which thermal variations cause mechanical effects.

The cylinder has cross section occupying the region $\Omega = \{(x, y) : r_0^2 \leq x^2 + y^2 \leq R^2\}$ with inner and outer radii $r_0 = 10$ mm and $R = 20$ mm, respectively. A zero heat flux boundary condition is maintained on the inner wall, while the outer wall is kept at the reference temperature Θ_0. The inner wall is dynamically prescribed a radial displacement of 1 mm per second, while the outer wall is mechanically free.

The problem is analysed for 20 seconds until the inner wall reaches a radius of $r = 3r_0$. The time-DG finite element mesh consists of trilinear shape functions with 56 elements around the circumference of the cylinder by 8 elements radially with one element thickness in the temporal direction with step length $\Delta t = 0.1$ s for each space-time slab. In this quasi-static case, since only the thermal equations contains temporal derivatives, the thermal fields are allowed to be discontinuous while the displacement field is continuous across the interfaces of each space-time slab. This implies that the numerical dissipation comes from the weak enforcement of the continuity of the thermal fields only.

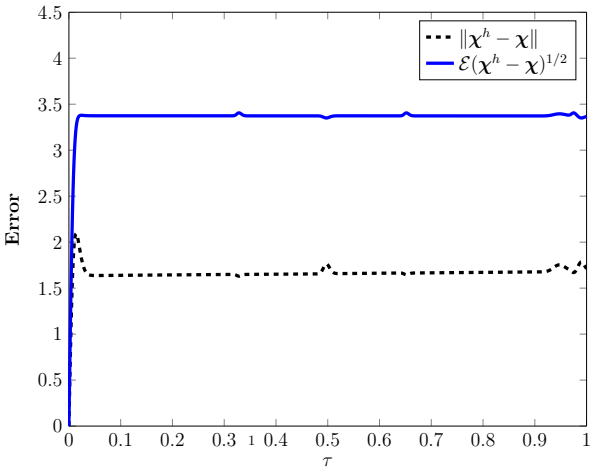

(a) Monolithic

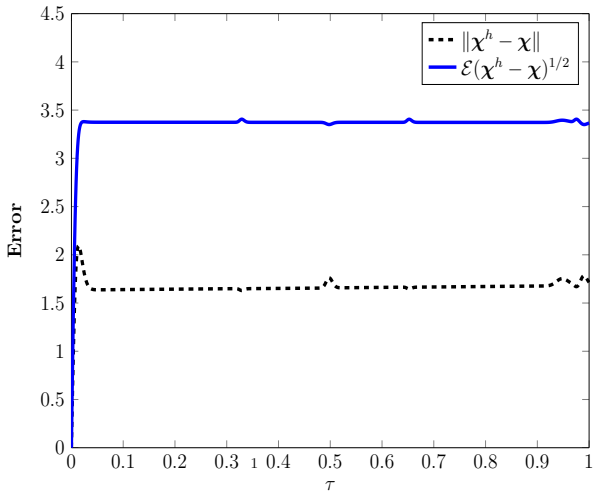

(b) Splitting

Figure 4: Propagation of laser pulse in type II thermoelasticity: the H^1-Energies and L^2-norms corresponding to using monolithic and splitting approaches.

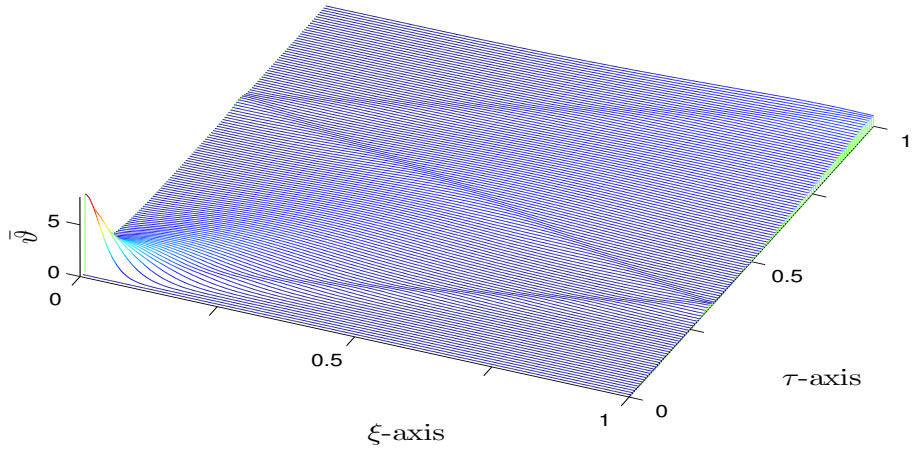

(a) Monolithic

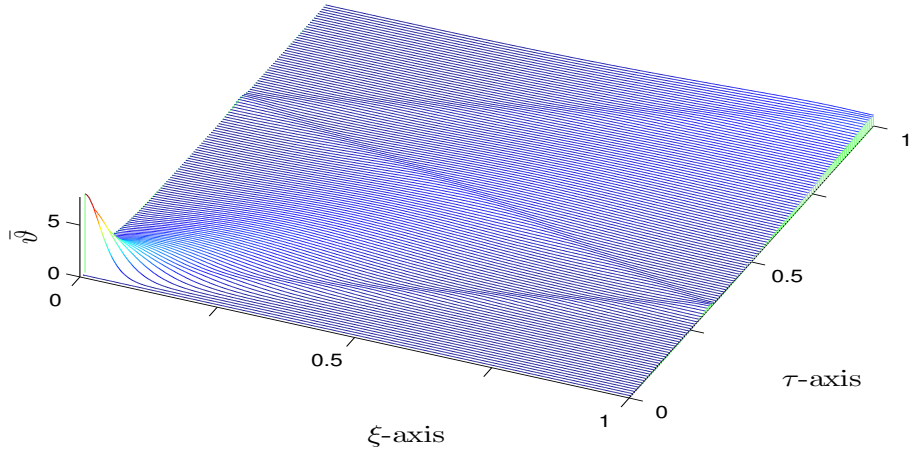

(b) Splitting

Figure 5: Propagation of laser pulse in type III thermoelasticity: temperature profile of the rod over the time period with $k = 0.1$, $\varepsilon_1 = 9$, $\varepsilon_2 = 0.5$, and $\Delta\xi = \Delta\tau = 0.001$

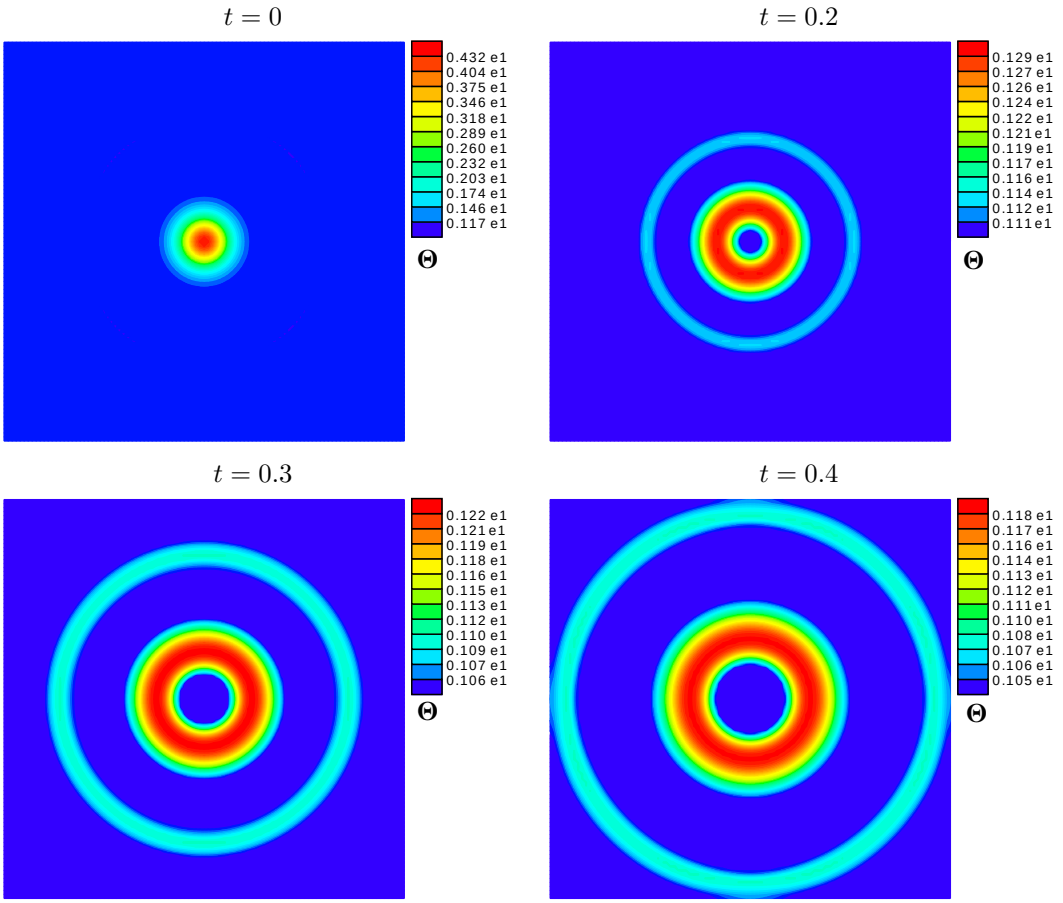

Figure 6: Temperature distribution in a square plate according to type III thermoelasticity where an initial pulse localized in space is initiated at the center.

Table 1: Initial pulse propagation: material properties

Speed of first sound	$\sqrt{E/\rho}$	1.96
Speed of second sound	$\sqrt{\kappa_2/\rho c}$	0.65
Conductivity ratio	κ_2/κ_3	100

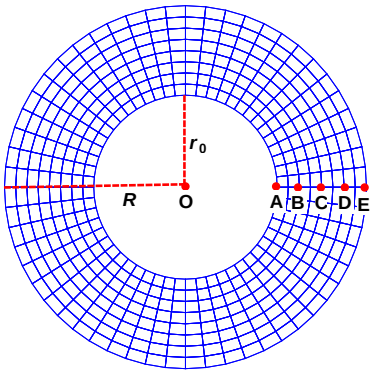

Figure 7: Finite element mesh for the problem of expansion of a thick-walled cylinder.

We consider two cases: the first is classical or type I thermoelasticity with $k_3 = 45$ N/sK and the other is type III thermoelasticity with $k_2 = 90$ N/K and $k_3 = 30$ N/sK.

Fig. 8 shows temperature variations over time for each case sampled at the equally spaced points along the radial direction labeled A-E as shown in the Fig. 7. As expected, in both cases, the temperature of the entire cylinder is converging to the reference temperature as time increases. The sinusoidal thermal response of type III is due to a temperature wave moving back and forth indicating second sound phenomenon.

6. Conclusion

An operator-splitting strategy coupled with a space-time discontinuous Galerkin finite element method for the solution of the transient and fully-coupled initial-boundary problem of generalized thermoelasticity was presented. Well-posdeness of the problem in the general setting (type III) is proven using the theory of semigroups. The defining operator is split additively so that the first sub-operator represents an isentropic (adiabatic) elasticity in which the entropy density is held fixed, and the other is a non-standard heat conduction at fixed configuration. Both of the sub-problems are also shown to inherit the same contractivity property as the full problem.

Each sub-problem is then discretised separately using a time-discontinuous Galerkin finite element method where the unknown fields are allowed to be discontinuous along the interfaces of each space-time slab. Weak continuity of the unknown fields is enforced using an L^2-inner product which differs from the original time-discontinuous formulation using an energy-inner product presented in [15, 16] which was formulated for linear elastodynamics problem. The unconditional stable behaviour of each of the algorithms is proven without the need to add extra 'artificial viscosity'. The algorithm for the global problem is finally obtained by way of Lie-Trotter-Kato product formula, leading to an unconditional stable scheme.

The results presented in this paper are demonstrated by a number of numerical examples in both one and two dimensions. The efficiency of the current numerical scheme were examined by comparing the rate of convergence with the corresponding monolithic approach. The splitting scheme performs well in low-order approximations, such as Q1, with better efficiency compared to the monolithic scheme. However, the result clearly demonstrated that the efficiency of the splitting scheme does not scale up in the same way as we go to higher-order approximation, for example Q2. The capability of the splitting algorithm is tested using problems involving propagation of heat waves driven by a pulsing laser heat source and an initial temperature disturbance in one and two dimensions respectively. Furthermore, the capability of the non-standard thermoelasticity and the proposed numerical method to model the phenomenon of second sound in some solids is demonstrated by considering the quasi-static expansion of an infinitely long thick walled cylinder in plane stress.

The DG formulation proposed in this work may be extended to the non-linear regime without the need to eliminate the displacement-velocity relation in the formulation. Hence, a full recovery of the numerical

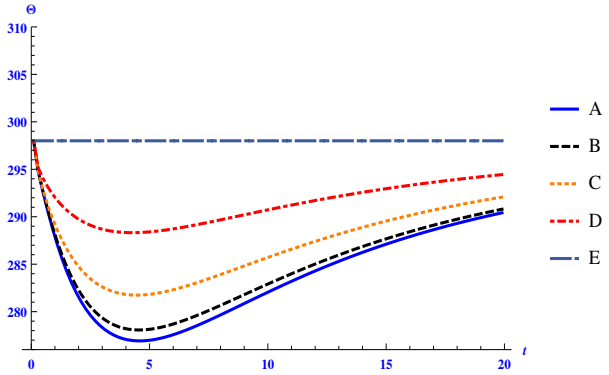

(a) **Type I**

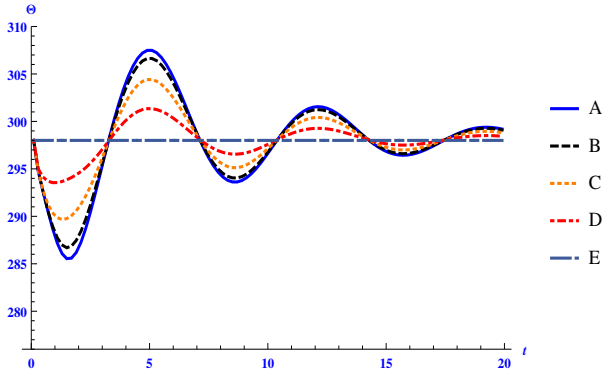

(b) **Type III**

Figure 8: Temperature profile of five points in the cylinder which are 0 mm, 2.5 mm, 5 mm, 7.5 mm, and 10 mm away from the inner wall and shown with the labels A, B, C, D, and E.

dissipation in the non-linear case is possible. This will be the subject of a forthcoming work in which issues such as non-linear stability and the existence of Lyapunov function are discussed.

Acknowledgments. The work reported in this paper has been supported by the National Research Foundation of South Africa through the South African Research Chair in Computational Mechanics. This support is acknowledged with thanks. The authors also thank Professor S. Bargmann for discussions which led to various improvements in the work.

References

[1] W. Dreyer, H. Struchtrup, Heat pulse experiments revisited, Continuum Mechanics and Thermodynamics 5 (1993) 3–50.
[2] G. Caviglia, A. Morro, B. Straughan, Thermoelasticity at cryogenic temperatures, International Journal of Nonlinear Mechanics, 27(2) (1992) 251-263.
[3] M. J. Freyer, H. Struptrup, Moment model and boundary conditions for energy transport in the phonon gas, Continuum Mechanics and Thermodynamics (2013) 1–26
[4] R. B. Hetnarski, J. Ignaczak, Generalized thermoelasticity, Journal of Thermal Stresses 22 (1999) 451–476.
[5] B. Straughan, Heat waves, Springer Science and Business Media, 2011.
[6] A. E. Green, P. M. Naghdi, A re-examination of the postulates of thermomechanics, Proceedings of the Royal Society of London Series A 423 (1991) 171–194.
[7] A. E. Green, P. M. Naghdi, On undamped heat waves in an elastic solid, Journal of Thermal Stresses 15 (1992) 253–264.
[8] A. E. Green, P. M. Naghdi, Thermoelasticity without energy dissipation, Journal of Elasticity 31 (1993) 189–208.
[9] A. E. Green, P. M. Naghdi, A new thermoviscous theory of fluids, Journal of Non-Newtonian Fluid Mechanics 56 (1995) 289–306.
[10] S. Bargmann, Remarks on the Green–Naghdi theory of heat conduction, Journal of Non-Equilibrium Thermodynamics 38 (2013) 101–118.
[11] D. S. Chandrasekharaiah, Thermoelasticity with second sound: a review, Applied Mechanics Reviews 39 (1996) 355–376.
[12] D. S. Chandrasekharaiah, Hyperbolic thermoelasticity: A review of recent literature, Applied Mechanics Reviews 51 (1998) 705–729.
[13] S. Bargmann, P. Steinmann, P. Jordan, On the propagation of second-sound in linear and nonlinear media: Results from green–naghdi theory, Physics Letters A 372 (2008) 4418–4424.
[14] R. Quintanilla, Existence in thermoelasticity without energy dissipation, Journal of Thermal Stresses 25 (2002) 195–202.
[15] G. Hulbert, T. J. R. Hughes, Space-time finite element methods for second-order hyperbolic equations, Computer Methods in Applied Mechanics and Engineering 84 (1990) 327–348.
[16] T. J. R. Hughes, G. M. Hulbert, Space-time finite element methods for elastodynamics: formulation and error estimates, Computer Methods in Applied Mechanics and Engineering 66 (1988) 339–363.
[17] B. Cockburn, C. W. Shu, Runge–Kutta discontinuous galerkin methods for convection-dominated problems, Journal of Scientific Computing, Kluwer Academic Publishers-Plenum Publishers 16 (2001) 173–261.
[18] D. K. Khalmonova, F. Costanzo, A space-time discontinuous galerkin finite element method for fully coupled linear thermo-elasto-dynamic problems with strain and heat flux discontinuities, Computer Methods Applied Mechanics and Engineering 197 (2008) 1323–1342.
[19] S. Bargmann, P. Steinmann, Theoretical and computational aspects of non-classical thermoelasticity, Computer Methods in Applied Mechanics and Engineering 196 (2006) 516–527.
[20] F. Armero, J. C. Simo, A new unconditionally stable fractional step method for non-linear coupled thermomechanical problems, International Journal for Numerical Methods in Engineering 35 (1992) 737–766.
[21] S. Bargmann, P. Steinmann, Modeling and simulation of first and second sound in solids, International Journal of Solids and Structures 45 (2008) 6067–6073.
[22] S. Bargmann, A. Favata, P. Podio-Guidugli, A revised exposition of the Green–Naghdi theory of heat propagation, Journal of Elasticity 114(2) (2014) 143–154.
[23] A. J. Chorin, T. J. R. Hughes, M. F. McCracken, J. E. Marsden, Product formulas and numerical algorithms, Communications on Pure and Applied Mathematics 31 (1978) 205–256.
[24] H. Holden, K. H. Karlsen, K. Lie, N. H. Risebro, Splitting methods for partial differential equations with rough solutions: Analysis and MATLAB programs, European Mathematical Society, 2010.
[25] J. C. Simo, Nonlinear stability of the time-discrete variational problem of evolution in nonlinear heat conduction, plasticity and viscoplasticity, Computer Methods in Applied Mechanics and Engineering 88 (1991) 111–131.
[26] C. Johnson, Discontinuous Galerkin finite element methods for second order hyperbolic problems, Computer Methods in Applied Mechanics and Engineering 107 (1993) 117–129.
[27] S. T. Miller, R. B. Haber, A spacetime discontinuous galerkin method for hyperbolic heat conduction, Computer Methods in Applied Mechanics and Engineering 198(2) (2008) 194–209.
[28] The MathWorks Inc., MATLAB, Version 8.01.0.604 (R2013a), Natick, Massachusetts (2013).
[29] Wolfram Research, Inc. Mathematica, Version 10.1, Wolfram Research, Inc., Champaign, Illinois (2015).
[30] J. Korelc, Multi-language and multi-environment generation of nonlinear finite element codes, Engineering with Computers 18(4) (2002) 312–327.
[31] A. Kuzmin, M. Luisier, O. Schenk, Fast methods for computing selected elements of the Greens function in massively

parallel nanoelectronic device simulations. In F. Wolf, B. Mohor, and D. Mey, editors, Euro-par 2013 Parallel Processing, Lecture Notes in Computer Science, Springer Berlin Heidelberg. 8097 (2013) 533–544.

[32] O. Schenk, K. Gärtner. Solving unsymmetric sparse linear equaitions with Pardiso, Journal of Future Generation Computer Systems, 20(3) (2004) 275–487.